Simulation of a two-dimensional, N=2 supersymmetric lattice gauge theory

Thesis towards partial fulfillment of the degree "Master of Science" (M.Sc.) in Physics

Submitted by Suraj Krishnamurthy, born on 01.01.1989 in Bangalore, India.

1st supervisor: Prof. Dr. Andreas Wipf, TPI, Jena

2nd supervisor: Dr. Björn-Hendrik Wellegehausen, ITP, Gießen

Contents

1. Introduction

The Standard Model is the bulwark of particle physics today. Two of the main guiding principles that have been used in the formulation of the framework are those of symmetry and gauge invariance. Along with the symmetries of space-time, i.e. Poincaré symmetry, internal symmetries play a very important role in describing physical phenomena. The model unifies three of the four fundamental interactions in the local gauge group $SU(3)$ x $SU(2)$ x $U(1)$. Gravity is yet to be unified and research is ongoing to this end. These considerations are responsible for the remarkable success of the Model, most of which has been rigorously tested over the last 30-40 years[1–4].

The Standard Model, nevertheless, does not explain many features of nature: neutrino oscillations[5], baryon asymmetry[6], gravity, dark matter & energy[7] and the gauge-hierarchy problem to name some. It is now thought of as an effective field theory, valid only until a certain energy limit (of about 1 TeV). Solving the outstanding problems has prompted many Beyond the Standard Model (BSM) theories, such as supersymmetry, string theory and loop quantum gravity.

Supersymmetry (SUSY) is an oft-used extension of the Standard Model. It is, mathematically, the only possible extension of Poincaré symmetry[8,9], and postulates fermionic "superpartners" for all bosons and vice-versa. One objective of the experiments at the Large Hadron Collider (LHC) is to directly or indirectly detect signatures of such supersymmetric particles, but as of now, none have been found. If SUSY is to be a symmetry of nature, it must thus be spontaneously broken at the energy scales that are currently accessible. Supersymmetric theories provide answers, or at least hints to some of the problems of the Standard Model, such as the gauge-hierarchy problem, strong CP violation and the unification of all interactions[10,11]. They also provide candidate particles for dark matter[12,13], making them very fruitful areas of study.

Many aspects of quantum field theories cannot be studied using perturbation theory. The phenomenon of confinement in QCD is a prime example. The best way to study them non-perturbatively is using the techniques of lattice field theory, which was first thought of by Wilson[14]. Monte Carlo simulations of QCD on the lattice have enjoyed much success[15]. There are many considerations to be taken when putting field theories on the lattice; more so if the theory is

supersymmetric. It is well-known that the Leibniz rule fails on the lattice[16]. Since SUSY is a space-time symmetry, it is explicitly broken on the lattice. The gluino condensate is the only SUSY-breaking quantity and so, it is preferable to use lattice formulations for fermions that are chiral. Coupled with the Nielsen-Ninomiya no-go theorem[17], which states that local, real, free fermions, having chiral and translational invariance on the lattice, must undergo doubling, we have a few options for the fermion formulation. The way out of the no-go theorem is to violate at least one of the assumptions. The optimal choice would be the Ginsparg-Wilson formulation[18], which maintains an exact chiral symmetry, but breaks it ultra-locally. It is also computationally intensive. The Wilson formulation (which breaks chiral symmetry explicitly), being less demanding, can also be used, along with a tuning of the gluino mass.

The present work studies a dimensionally-reduced version of the N=1 SYM theory in 4 dimensions, with a focus on the restoration of supersymmetry in the continuum limit. The investigation is done using the Euclidean, lattice formulation of the theory and simulating it using Monte Carlo techniques. It is organized as follows: in the next section, a brief overview of supersymmetry is given, followed by the superfield formalism and the formulation of supersymmetrical Yang-Mills theories using it. Section 3 covers the basics of lattice gauge theories, how to put fields on the lattice, particularly, and a brief section on error sources and the methods used to reduce them. Section 4 explains the different algorithms used in this work. In section 5, the theory under consideration is obtained via dimensional reduction of the N=1 SYM theory in 4 dimensions. The simulation results are presented in section 6. A few very interesting aspects of the theory presented themselves during the simulations. These are discussed along with a summary of the results and an outlook of possible future investigations in section 7.

2

2. Supersymmetrical Yang-Mills theories

2.1. A brief foray into supersymmetry

A space-time symmetry between bosons and fermions was independently discovered by Gervais & Sakita[19], Golfand & Likhtman[20] in 1971 and Volkov & Akulov in 1972[21]. A couple of years later, Wess & Zumino understood the renormalization properties of such theories[22] and, along with Salam, began figuring out particle physical applications. The Standard Model was then extended with supersymmetry by Georgi & Dimopoulos in 1981, leading to the Minimal Supersymmetric Standard Model (MSSM)[10].

As with any continuous symmetry, our first instinct should be to find the charges/generators of the symmetry, or more importantly, the algebra obeyed by these generators. The SUSY charges ("supercharges") are usually represented by Q_α, $\alpha = 1...4N$. The charges can then be grouped into a 2-component Weyl spinor:

$$Q_\alpha = \begin{pmatrix} Q_A \\ \bar{Q}_{\dot{A}} \end{pmatrix} \tag{1}$$

The algebra obeyed by the charges is:

$$[Q_A, M^{\mu\nu}] = (\sigma^{\mu\nu})_A^B Q_B \qquad\qquad [\bar{Q}_{\dot{A}}, M^{\mu\nu}] = (\bar{\sigma}^{\mu\nu})_{\dot{A}}^{\dot{B}} \bar{Q}_{\dot{B}}$$

$$[Q_A, P^\mu] = 0 \qquad\qquad [\bar{Q}_{\dot{A}}, P^\mu] = 0$$

$$\{Q_A, Q_B\} = 0 \qquad\qquad \{\bar{Q}_{\dot{A}}, \bar{Q}_{\dot{B}}\} = 0 \tag{2}$$

$$\{Q_A, \bar{Q}_{\dot{B}}\} = 2(\sigma^\mu)_{A\dot{B}} P_\mu$$

Thus, the effect of two simultaneous supersymmetry transformations is a displacement. The action of the supercharges on a state is to change its helicity by one-half, thus turning bosons into fermions and vice-versa. Further, the particles in a "supermultiplet" have the same four-momentum because the supercharges and the momentum operator commute. If SUSY is unbroken, the particles must also have the same mass. Since there have been no observations of the such mass-degenerate partners, SUSY must be spontaneously broken at currently accessible energies.

Many of the supersymmetric theories that are studied are extensions of non-abelian gauge theories. Such theories have massless exchange particles and hence massless supermultiplets. Let us take a look at the massless representations. Consider a massless one-particle state. The frame of reference can always be shifted to one where the four-momentum is:

$$P_\mu = (E, 0, 0, E) \tag{3}$$

The properties of the state are completely specified by its energy E and helicity h. In this frame:

$$\sigma^\mu P_\mu |E, h\rangle = (P^0 \sigma^0 - P^3 \sigma^3) |E, h\rangle = \begin{pmatrix} 0 & 0 \\ 0 & 2P^0 \end{pmatrix} |E, h\rangle \tag{4}$$

Assuming, for simplicity, the case with 1 supersymmetry ($N=1$) and using the relation

$$\{Q_A, \bar{Q}_{\dot{B}}\} = 2(\sigma^\mu)_{A\dot{B}} P_\mu \tag{5}$$

this leads to:

$$\{Q_1, \bar{Q}_{\dot{1}}\} |E, h\rangle = \{Q_1, \bar{Q}_{\dot{2}}\} |E, h\rangle = \{Q_2, \bar{Q}_{\dot{1}}\} |E, h\rangle = 0 \tag{6}$$

whereas

$$\{Q_2, \bar{Q}_{\dot{2}}\} |E, h\rangle = 4P^0 |E, h\rangle \tag{7}$$

Using the first commutation relation in (6) and keeping in mind that physical states with positive definite norm must be considered, one reaches the conclusion:

$$Q_1 = \bar{Q}_{\dot{1}} = 0 \tag{8}$$

and one need be concerned with the Q_2s only.

Performing the rescaling:

$$q_2 = \sqrt{4P^0} \, Q_2 \tag{9}$$

(and a corresponding rescaling of the conjugate), (8) reduces to:

$$\{q_2, \bar{q}_{\dot{2}}\} = 1 \tag{10}$$

An irreducible representation of this Clifford algebra can be characterized by a ground state such that:

$$q_2 |E, h_0\rangle = 0 \tag{11}$$

Other states are then built by the action of the other charge:

$$\bar{q}_{\dot{2}} |E, h_0\rangle = \left| E, h_0 + \frac{1}{2} \right\rangle \tag{12}$$

4

Although this is all there is for *N*=1 (along with the states demanded by CPT invariance), for a theory with an arbitrary number of supersymmetries labeled by *i*=1...N,

$$\bar{q}_{\dot{1}}\bar{q}_{\dot{2}}...\bar{q}_{\dot{N}}\left|E,h_0\right\rangle=\left|E,h_0+\frac{N}{2}\right\rangle \tag{13}$$

Any further application of a $\bar{q}$ will annihilate the state and a theory will have the following spectrum, easily obtainable from the binomial co-efficients (adapted from [23]):

Helicity	h_0	h_0+1/2	h_0+1	...	h_0+N/2
Number of states	$\binom{N}{0}=1$	$\binom{N}{1}=N$	$\binom{N}{2}$	...	$\binom{N}{N}=1$

However, caution should be exercised. The number of supersymmetry generators cannot be arbitrarily large. Since the number of components of a spinor increases quickly with the number of space-time dimensions,

$$dim(spinor)=integer\left(2^{(d-1)/2}\right) \tag{14}$$

and every generator constrains a theory, one cannot go to arbitrarily high dimensions without trivializing the theory. It has been shown that the maximum space-time dimensionality that allows for a non-trivial theory with interactions and no negative probabilities is 11[24]. The resulting supersymmetric theory contains 32 real supercharges.

2.2. Formulation of Supersymmetrical Yang-Mills (SYM) theories

If a supersymmetric theory is to describe the physical world, it must be a gauge theory. There are principally two different ways of formulating such theories. One could write the most general, renormalizable Lagrangians that are real and Lorentz-invariant and then tweak them and try to make them invariant under SUSY. This approach is perfectly valid, but is quite inelegant when compared to using the superspace formalism, which makes the construction "easier".

2.2.1. Superspace and superfields

In the case of "normal" space-time symmetries (such as invariance under translations or

rotations), the symmetry charges can be written as differential operators acting on the fields instead of functions of the fields. At first glance, this approach would seem to be ruled out for the supercharges, since the action of a supercharge on a state yields another state at the same point (second row of (2)). The anticommutator of supercharges, however, produces the same field at a displaced space-time point (fourth row of (2)). This suggests that the supercharges could be set up as differential operators, not on ordinary space-time, but on an extended space-time, called superspace. The superspace formalism was introduced by Salam & Strathdee in 1974[25].

In order to get a feel for the formalism, let us examine an example of a symmetry charge in regular space-time, the four-momentum P_μ. The (unitary) transformation corresponding to the charge is:

$$U(a) = \exp(i a^\mu P_\mu) \tag{15}$$

The parameter a^μ is the infinitesimal displacement four-vector and it is part of the argument of the transformed field, i.e.:

$$\varphi(x') = U(a)\varphi(x)U^\dagger(a) = \varphi(x^\mu + a^\mu) \tag{16}$$

Thus, if one starts with a field at a defined origin, a displacement of the field to the point x^μ can be achieved using the above operation with x^μ as the parameter. This is what is done in the superspace formalism.

Superspace is an extended space-time possessing four Grassmann co-ordinates in addition to the four commuting co-ordinates of regular space-time. The Grassmann co-ordinates are usually grouped into a two-component Weyl spinor and its Hermitian conjugate:

$$\begin{aligned} \theta &= \begin{pmatrix} \theta_1 \\ \theta_2 \end{pmatrix} \\ \bar{\theta} &= \begin{pmatrix} \bar{\theta}^{\dot{1}} \\ \bar{\theta}_{\dot{2}} \end{pmatrix} \end{aligned} \tag{17}$$

The fields are then dependent on all eight co-ordinates and are termed superfields:

$$Superfield\ \Phi = \Phi(x, \theta, \bar{\theta}) \tag{18}$$

There is then an expression analogous to (16):

$$U(a, \epsilon, \bar{\epsilon}) \Phi(x, \theta, \bar{\theta}) U^\dagger(a, \epsilon, \bar{\epsilon}) = \Phi(x', \theta', \bar{\theta}') \tag{19}$$

6

where ε & $\bar{ε}$ are the infinitesimal Grassmann parameters. The expressions for the transformed co-ordinates x', $θ'$ & $\bar{θ}'$ are:

$$x'^{\mu} = x^{\mu} + a^{\mu} + i\,\epsilon\,\sigma^{\mu}\bar{\theta} - i\,\theta\,\sigma^{\mu}\bar{\epsilon}$$

$$\theta' = \theta + \epsilon \tag{20}$$

$$\bar{\theta}' = \bar{\theta} + \bar{\epsilon}$$

Performing a Taylor expansion on a general superfield gives:

$$\Phi(x,\theta,\bar{\theta}) = f(x) + \theta.\varphi(x) + \bar{\theta}.\bar{\chi}(x) + (\theta.\theta)m(x) + (\bar{\theta}.\bar{\theta})n(x) + \theta\sigma^{\mu}\bar{\theta}v_{\mu}(x)$$

$$+ (\theta.\theta)(\bar{\theta}.\bar{\lambda}(x)) + (\bar{\theta}.\bar{\theta})(\theta.\psi(x)) + (\theta.\theta)(\bar{\theta}.\bar{\theta})d(x) \tag{21}$$

Since the action is a scalar under Lorentz transformations, the superfield must also be a scalar. This enables a deduction of the behavior of the various component fields: *f(x), m(x), n(x) & d(x)* are complex scalars, *φ(x), χ(x), λ(x) & ψ(x)* are Weyl spinors and $v_{\mu}(x)$ is a complex vector field. Each complex scalar contributes 2 bosonic degrees of freedom and the vector field contributes 8. Each Weyl spinor contributes 4 fermionic degrees of freedom, so there are 16 bosonic and 16 fermionic field components. The equality should be reassurance that the content is supersymmetric. This is a reducible representation of the superfield, whereas we usually require irreducible representations. These are obtained by placing constraints on the superfield.

2.2.2. Constrained superfields

The problem of superfields containing more components than is acceptable for irreducible representations was solved by Ferrara, Zumino & Wess[26]. There are three major ways to constrain superfields: using SUSY-covariant derivatives so that:

$$D_{A}\Phi = 0 \qquad \text{or} \qquad \bar{D}_{\dot{A}}\Phi = 0 \tag{22}$$

or apply a reality condition:

$$\Phi^{\dagger} = \Phi \tag{23}$$

The reality condition is the most relevant to this work, but we shall make a small detour to flesh out some details of the derivative constraints.

- **Chiral and anti-chiral superfields**

Differential operators which commute with the SUSY charges can be used to constrain equations which are invariant under SUSY. Such operators obey:

$$\{D_A, Q_B\} = \{\bar{D}_{\dot{A}}, Q_B\} = \{D_A, \bar{Q}_{\dot{B}}\} = \{\bar{D}_{\dot{A}}, \bar{Q}_{\dot{B}}\} = 0 \tag{24}$$

The explicit form of the SUSY-covariant derivatives is:

$$D_A = \frac{\partial}{\partial \theta^A} + i(\sigma^\mu \bar{\theta})_A \partial_\mu$$

$$\bar{D}_{\dot{A}} = -\frac{\partial}{\partial \bar{\theta}^{\dot{A}}} + i(\tilde{\sigma}^\mu \bar{\theta})_{\dot{A}} \partial_\mu \tag{25}$$

They also satisfy:

$$\{D, \bar{D}\} = -2i\sigma^\mu \partial_\mu$$

$$\{D, D\} = \{\bar{D}, \bar{D}\} = 0 \tag{26}$$

A chiral superfield satisfies the condition $\bar{D}_A \Phi = 0$. This implies:

$$\bar{\chi}(x) = 0 \qquad n(x) = 0 \qquad \psi(x) = 0$$

$$v_\mu(x) = -i\partial_\mu f(x) \qquad \bar{\lambda}(x) = \frac{i}{2}(\partial_\mu \varphi(x)\sigma^\mu) \qquad d(x) = -\frac{1}{4}\partial^\mu \partial_\mu f(x) \tag{27}$$

Therefore:

$$\Phi_{chiral} = f(x) + \theta . \varphi(x) + (\theta . \theta) m(x) - i(\theta \sigma^\mu \bar{\theta}) \partial_\mu f(x)$$

$$+ \frac{i}{2}(\theta . \theta)(\partial_\mu \varphi(x)\sigma^\mu \bar{\theta}) - \frac{1}{4}(\theta . \theta)(\bar{\theta} . \bar{\theta}) \partial^\mu \partial_\mu f(x) \tag{28}$$

The anti-chiral superfield, which satisfies $D_A \Phi^\dagger = 0$ can be obtained via a complex conjugation of the chiral superfield.

- **Vector/real superfields**

The appropriately named real superfield is obtained by enforcing the reality condition of a general superfield.

This constrains the component fields:

$$f^*(x) = f(x) \qquad m^*(x) = n(x) \qquad n^*(x) = m(x) \qquad d^*(x) = d(x)$$

$$\chi(x) = \varphi(x) \qquad \lambda(x) = \psi(x) \qquad v_\mu^*(x) = v_\mu(x)$$

(29)

The degrees of freedom are halved, from 16 each of bosons & fermions to 8 each. Since one of the component fields is a vector field (which facilitates the supersymmetric generalization of a gauge vector field), real superfields are also called vector superfields. Using the Wess-Zumino gauge to eliminate some of the component fields, one arrives at the simplest form of the vector superfield:

$$V(x,\theta,\bar{\theta}) = -(\theta \sigma^\mu \bar{\theta}) v_\mu(x) - i(\theta.\theta)(\bar{\theta}.\bar{\lambda}(x)) + i(\bar{\theta}.\bar{\theta})(\theta.\lambda(x))$$

$$-\frac{1}{2}(\theta.\theta)(\bar{\theta}.\bar{\theta}) d(x)$$

(30)

where $d(x)$ is a now a minor redefinition of the earlier field. In this gauge, the normal gauge freedom of $v_\mu(x)$ is preserved. Further, the components $\lambda(x)$ (and $\bar{\lambda}(x)$) and $d(x)$ are invariant under super gauge transformations. As will be seen in the following sections, the fermionic components $\lambda(x)$ and $\bar{\lambda}(x)$ will form the spin-1/2 superpartner of the gauge field, called a gaugino.

The scalar field $d(x)$ is an auxiliary degree of freedom. It will have no kinetic term in the Lagrangian and is eliminated using its equation of motion.

2.2.3. Constructing supersymmetric gauge theories

The most general supersymmetric Lagrangian that can be formed using these three kinds of superfields, chiral, anti-chiral & vector, is:

$$L = \frac{1}{4g^2} Tr[((W^A W_A) + h.c.)_F] + (\Phi^\dagger e^V \Phi)_D + (\frac{1}{2} m_{ij} \Phi_i \Phi_j + \frac{1}{2} y_{ijk} \Phi_i \Phi_j \Phi_k + h.c.)_F$$

(31)

A clarification of the terms is perhaps in order.

• W^A is the supersymmetric generalization of the field strength tensor. It is formed out of the vector field and the SUSY-covariant derivatives:

$$W_A = -\frac{1}{4}(\bar{D}.\bar{D}) e^{-V} D_A e^V$$

(32)

• The subscripts $(...)_D$ and $(...)_F$ represent the D- and F-terms. These are the highest non-zero co-

9

efficients of the corresponding superfield when it is expanded as a function of θ and $\bar{\theta}$. Specifically, $(...)_F=(...)|_{\theta\theta\bar{\theta}\bar{\theta}}$ and $(...)_D=(...)|_{\theta\theta,y\to x}$. These terms only contribute a total divergence under SUSY transformations, so such terms are exactly what is needed in the Lagrangian.

• The co-efficient m_{ij} has dimension 1. It is a necessary addition to obtain a Lagrangian with the correct dimensions: each superfield has dimension 1. The projection of the F-term, which involves the Grassmann infinitesimals $d\theta_1$ and $d\theta_2$, also has dimension 1 since each Grassmann variable has dimension ½, leading to a total of 3. A similar analysis yields the fact that y_{ijk} is dimensionless.

2.2.4. The *N*=1 SYM Lagrangian in 4D

The 4-dimensional *N*=1 SYM is the starting point of this work and we now have all the tools necessary to construct it in the continuum. In order to write the Lagrangian, all that is needed is the first term in (31), namely:

$$L=\frac{1}{4g^2}Tr\left[\left(\left(W^A W_A\right)+h.c.\right)_F\right]$$
(33)

To make things simpler, one may use the form of W_A in terms of the components of the vector superfield:

$$W_A^a=\sqrt{2}\lambda_A^a-d^a\theta_A-\left(\sigma^{\mu\nu}\theta\right)_A F_{\mu\nu}^a+\frac{i}{\sqrt{2}}\left(\theta.\theta\right)\left(\sigma^{\mu}D_{\mu}\bar{\lambda}^a\right)_A$$
(34

Performing the contraction and extracting the F-terms, we obtain the final result:

$$L=Tr\left(-\frac{1}{4}F_{\mu\nu}F^{\mu\nu}+\frac{i}{2}\bar{\lambda}\gamma_{\mu}D^{\mu}\lambda\right)$$
(35)

$F^{\mu\nu}$ is the regular field strength tensor:

$$F_{\mu\nu}=\partial_{\mu}A_{\nu}-\partial_{\nu}A_{\mu}-ig\left[A_{\mu},A_{\nu}\right]$$
(36)

A_{μ} is the gauge field transforming according to the adjoint representation of the gauge group and g is the (dimensionless) coupling constant. λ is a Majorana spinor in the adjoint representation. The covariant derivative has the usual definition in the adjoint:

$$D_{\mu}\lambda=\partial_{\mu}\lambda-ig\left[A_{\mu},\lambda\right]$$
(37)

The Lagrangian is invariant under the SUSY transformations:

$$\delta_\epsilon A_\mu = i\bar{\epsilon}\,\gamma_\mu\lambda \qquad \delta\lambda = i\,\sigma_{\mu\nu}F^{\mu\nu}\epsilon \qquad \delta\bar{\lambda} = -i\,\bar{\epsilon}\,\sigma_{\mu\nu}F^{\mu\nu} \tag{38}$$

It is especially clear from the transformations that SUSY transforms bosonic fields into fermionic ones and vice-versa. Further, because the Lagrangian is supersymmetric, the fermions have to transform in the same way as the bosons, namely under the adjoint representation of the gauge group (this is also the reason why one is able to write the fermionic part of (35) in the same way as the bosonic part).

It is evident that the Lagrangian is identical in form to the QCD Lagrangian:

$$L = Tr\left(-\frac{1}{4}F_{\mu\nu}F^{\mu\nu} + \frac{i}{2}\bar{q}\,\gamma_\mu D^\mu q\right) \tag{39}$$

but for a couple of differences. The fermionic q fields in QCD are Dirac fermions and they lie in the fundamental representation of the gauge group ($SU(3)$). In contrast, the theory represented by (35) contains Majorana fermions transforming under the adjoint action of the gauge group. It is this similarity in form (and properties), however, that warrants us calling it a QCD-like theory.

3. Lattice gauge theory

The essence of defining a field theory on a space-time lattice is, on the surface, simple: replace the derivatives in the Lagrangian with finite differences. In gauge theories, the gauge potential rotates the frame of reference in an internal symmetry space as we travel between space-time points. In transferring a gauge theory onto the lattice, the matter fields are assigned to the discrete latticized sites of space-time. Hence, displacements between neighboring sites are simply the links of the lattice. A unique element of the gauge group must be assigned to each of these links to understand the state of a system. The links must also be oriented, in the sense that if an element of the gauge group specifies a link in one orientation, the inverse element specifies the same link in the opposite orientation. The collection of these gauge group elements plays the role of the continuum gauge potential.

Calculations of observables using the lattice has its roots in the path integral formulation of quantum mechanics, so we will briefly recall the most relevant points before moving on to method of formulation of lattice theories.

3.1. Quantum mechanics and path integrals

The path integral formulation of quantum mechanics was perfected by Feynman[27], who built on the ideas of Dirac and Wiener. In the simplest of terms, it gives the amplitude for the displacement of a particle between two points as the sum over all possible paths (essentially an infinite number) between the points.

Consider the expression of the quantum mechanical amplitude for a particle in 1D to travel from point x at time t to the point x' at time t':

$$\langle x', t' | x, t \rangle = \langle x' | e^{-iH(t'-t)} | x \rangle \tag{40}$$

By inserting a complete set of co-ordinate eigenstates and dividing the time interval $T=t'-t$ into n equal parts, one obtains the path integral expression for the amplitude:

$$\langle x' | e^{-iHT} | x \rangle = \int Dx \, e^{iS/\hbar} \tag{41}$$

where

$$\int Dx = \prod_t \prod_i dx_i(t) \tag{42}$$

represents the integration over all possible paths for the general 3D case. *S* is the classical action and so, each path is weighed by the action evaluated along it.

3.2. Field theory and functional integrals

Consider, as an example, a scalar field $\varphi(\boldsymbol{x},t)$. It evolves in time according to:

$$\varphi(\boldsymbol{x},t) = e^{iHt} \varphi(\boldsymbol{x},t=0) e^{-iHt/\hbar} \tag{43}$$

Green's functions are very important observables in field theory because they essentially contain all required information about a system. They are written as the vacuum expectation values (vevs) of time-ordered products of field operators, such as:

$$\langle 0|\varphi(x_1)\varphi(x_2)...\varphi(x_n)|0\rangle \qquad t_1 > t_2 > ... > t_n \tag{44}$$

We can write the functional integral expression for Green's functions by constructing analogues to the quantities that arose in the quantum mechanical case:

$$x_i(t) \Leftrightarrow \varphi(\boldsymbol{x},t)$$

$$\prod_{t,i} dx_i(t) \Leftrightarrow \prod_{t,\boldsymbol{x}} d\varphi(\boldsymbol{x},t) \equiv D\varphi \tag{45}$$

The functional integral representation of a Green's function is then:

$$\langle 0|\varphi(x_1)\varphi(x_2)...\varphi(x_n)|0\rangle = \frac{1}{Z} \int D\varphi \, \varphi(x_1)\varphi(x_2)...\varphi(x_n) e^{iS/\hbar}$$

$$Z = \int D\varphi \, e^{iS/\hbar} \tag{46}$$

There is one problem with the formulation as it is. The imaginary exponents mean the integrands oscillate, leading to a convergence problem. To remedy this, we go over to imaginary time via a "Wick rotation".

13

3.3. Euclidean field theory

To perform a Wick rotation, the time components are replaced with an imaginary time via a rotation into the complex plane using $t \rightarrow -i\tau$.

This leaves the Green's functions in the form:

$$G_E(x_1, x_2, ..., x_n) = \frac{1}{Z} \int D\varphi \, \varphi(x_1) \varphi(x_2) ... \varphi(x_n) e^{-S_E}$$

$$Z = \int D\varphi \, e^{-S_E} \tag{47}$$

The reason for the nomenclature can be seen from an observation of the change in the space-time metric:

$$ds^2 = dx^2 + dy^2 + dz^2 - dt^2$$
$$\downarrow$$
$$ds^2 = dx^2 + dy^2 + dz^2 + d\tau^2 \tag{48}$$

The metric after a Wick rotation looks like a 4D generalization of the regular Euclidean metric of 3D space.

The use of the Wick rotation is clear from (47). The oscillations are now gone. Fields with a large action (strongly fluctuating fields) are heavily suppressed by the exponential factor. The largest contributions come from paths which are close to the classical path.

The original quantities of interest, the Green's functions in real time, are obtained from G_E by analytical continuation.

$$G(t_1, t_2) = G_E(it_1, it_2) \tag{49}$$

The continuation must be done so that all the time components are rotated simultaneously in the complex time-plane.
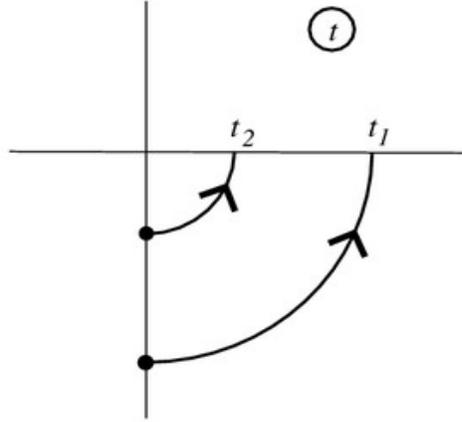
Fig. 3.1: Wick rotation from imaginary to real time co-ordinates (taken from [28])

There are a number of similarities between Euclidean field theory as it has been formulated and statistical mechanics. The following is adapted from [28].

Euclidean field theory	Statistical mechanics
Generating functional: $\int D\varphi \, exp(-S_E)$	Partition function: $\sum exp(-\beta H)$
Action: S	Hamilton function: βH
Mass m as: $G \sim e^{-m\tau}$	Inverse correlation length $1/\xi$ as: $G \sim e^{-x/\xi}$

These analogies allow many of the methods of statistical mechanics to be used while investigating Euclidean field theories. The square of the coupling constant in the field theory is also analogous to the temperature of a statistical system and, identifying strong coupling/weak coupling with high temperature/low temperature, expansions in these limits are regularly used, just as in statistical mechanics.

3.4. From the continuum to the lattice

Consider a hypercubic lattice of space-time specified by:

$$x_\mu = a\, n_\mu \qquad n_\mu \in \mathbb{Z} \tag{50}$$

a being the lattice spacing.

Matter degrees of freedom are then placed at the lattice sites, for eg.:

$$\psi(x) \rightarrow \psi(n) \qquad \bar{\psi}(x) \rightarrow \bar{\psi}(n) \tag{51}$$

Under gauge transformation, they vary as:

$$\psi(n) \rightarrow \Omega(n)\psi(n) \tag{52}$$

As mentioned earlier, the gauge fields live on the links of the lattice and possess an intrinsic direction. The field $U_\mu(n)$ is on the link between the lattice sites n and $n+\mu$ in the μ-direction. The variable $U_{-\mu}(n)$ is not independent of $U_\mu(n)$. They are related via:

$$U_{-\mu}(n) = U_\mu^\dagger(n-\hat{\mu}) \tag{53}$$

These "link variables" are not exact analogues of the continuum gauge fields, but are the lattice versions of the gauge transporter:

$$U_\mu(n) = \exp(ia A_\mu(n)) \tag{54}$$

They transform under gauge transformations as:

$$U_\mu(n) \rightarrow \Omega(n)U_\mu(n)\Omega^\dagger(n+\hat{\mu}) \tag{55}$$

The link variables $U_\mu(n)$ are group variables and are fundamental objects on the lattice.

Other changes that have to made on the lattice concern derivatives and integrals.

$$\partial_\mu \varphi(x) \rightarrow \Delta_\mu \varphi(n) \equiv \frac{1}{a}(\varphi(n+a\hat{\mu}) - \varphi(n))$$

$$\int d^4 x \rightarrow a^4 \sum_n \tag{56}$$

The discrete form of the derivative written (the forward difference) is, of course, one choice out of many. A choice of, for example, a backward difference or symmetrical difference can also be made. This freedom exists because the finite difference operator is an operator whose arguments are defined on the lattice sites and whose values are on the links. Therefore, there is no unique or natural way to represent it only on the sites.

3.4.1. Gauge fields on the lattice

In the continuum, the field strength $F_{\mu\nu}$ specifies the rotation of the reference frame for the

16

transport around an infinitesimal rectangular closed path with sides dx_μ & dy_μ. The analogous closed paths on the lattice are simply its smallest squares, which are called "plaquettes". An example of a transporter around a plaquette with vertices n_1, n_2, n_3 & n_4 would be:

$$U_{\mu\nu}(n) \equiv U_P = U_\mu(n) U_\nu(n+\hat{\mu}) U_\mu^\dagger(n+\hat{\nu}) U_\nu^\dagger(n) \tag{57}$$

From the purpose of the field strength as described above, one can see that $F_{\mu\nu}$ vanishes if the transport around the closed path leaves the reference frame unchanged, i.e. if it is the identity. As the values deviates away from the identity, larger positive values are taken. In the same way, one writes the lattice action as a function of a plaquette, such that, if $U_P = \mathbf{1}$, the action is zero. Just like the continuum behavior, larger deviations from **1** lead to larger positive values of the action. The total action can then be obtained by summing over all plaquettes of the lattice.

One form of the lattice gauge action is:

$$S_{gauge} = c_0 \beta \sum_{plaquette} \Re\left(Tr\, U_{plaquette}\right) + c_1 \beta \sum_{1x2\, rectangle} \Re\left(Tr\, U_{1x2\, rectangle}\right)$$
$$+ c_2 \beta \sum_{1x3\, rectangle} \Re\left(Tr\, U_{1x3\, rectangle}\right) \tag{58}$$

The co-efficients c_0, c_1 & c_2 take different values for different form of the action. $U_{plaquette}$ is the form written in (57) and is also written as $U_\square$ to represent an elementary square on the lattice. Similarly, $U_{1x2\, rectangle}$ & $U_{1x3\, rectangle}$ are terms that involve larger loops on the lattice: $U_{1x2\, rectangle} \equiv U_{\square\square}$ & $U_{1x3\, rectangle} \equiv U_{\square\square\square}$.

The simplest form of the gauge action is the Wilson action, named after Wilson[14]. The co-efficients take the values $c_0 = 1$, $c_1 = c_2 = 0$, leading to the form:

$$S_{Wilson} = \beta \sum_{plaquette} \Re\left(Tr\, U_{plaquette}\right) \tag{59}$$

The constant β is to be determined using the requirement that the usual Yang-Mills action should be recovered in the continuum limit. This leads to:

$$\beta = \frac{6}{g_{lattice}^2} \tag{60}$$

where $g_{lattice}$ is the bare coupling constant on the lattice.

Since, in practice, the lattice spacing is non-zero, discretization errors arise, which one should aim to minimize. An effective way to achieve this was established by Lüscher, Sint, Sommer & Weisz following a suggestion from Symanzik[29]. This form of the action, named the Symanzik action, takes

into account larger loops and is a closer approximation of the continuum. In the Symanzik action, the co-efficients take the values c_0=1- 8c_1, c_1=-1/12 & c_2=0. The Symanzik action is:

$$S_{Symanzik} = \frac{5\beta}{3} \sum_{plaquette} \Re\left(Tr\, U_{plaquette}\right) - \frac{\beta}{12} \sum_{1x2\,rectangle} \Re\left(Tr\, U_{1x2\,rectangle}\right) \tag{61}$$

This will be the gauge action used in this work.

Observables in the quantum theory can then be calculated using:

$$\langle A \rangle = \frac{1}{Z} \int \prod_b dU(b)\, A\, e^{-S}$$

$$Z = \int \prod_b dU(b)\, e^{-S} \tag{62}$$

The integration $dU(b)$ for the link b is an invariant integration over the manifold of the gauge group and is normalized to:

$$\int dU = 1 \tag{63}$$

With this, there is no necessity of gauge fixing. The total "volume of the gauge group" is unity.

This regularization is taken care of on the lattice by the space-time discretization. The analogous expression of (62) is:

$$\langle A \rangle = \frac{1}{Z} \sum_U A(U)\, e^{-S_{Symanzik}}$$

$$Z = \sum_U e^{-S_{Symanzik}} \tag{64}$$

Depending on whether the Us are elements of a discrete gauge group or a Lie group, the sums are ordinary sums or invariant integrals over the group manifold as discussed above.

3.4.2. Fermions on the lattice

When representing them on the lattice, one must keep in mind that fermions are represented by anticommuting Grassmann variables. Taking the familiar example of a Dirac field, it will have the anticommuting variables $\psi_\alpha(x)$ and $\bar{\psi}_\alpha(x)$, with α=1,2,3,4 being the Dirac index. The variables satisfy anticommutation relations such as:

$$\left\{\psi_\alpha(x), \psi_\beta(x)\right\}=0 \tag{65}$$

and so on.

A fermionic Green's function is of the form:

$$\langle 0|A|0\rangle=\frac{1}{Z}\int D\psi D\bar{\psi}A e^{-S_F} \tag{66}$$

where

$$D\psi D\bar{\psi}=\prod_x \prod_\alpha d\psi_\alpha(x)d\bar{\psi}_\alpha(x) \tag{67}$$

Calculating functional integrals with Grassmann variables is actually simple keeping this integration rule in mind:

$$\int d\eta_i(a+b\eta_i)=b \tag{68}$$

For an integral of the form:

$$\int D\psi D\bar{\psi}e^{-\int d^4x\,\bar{\psi}(x)D\psi(x)} \tag{69}$$

the rule (68) reduces this to *det(D)*. This is a general formula since any action which is bilinear in the fermionic fields can be put into the form in the exponential. *D* is called the fermion matrix/Dirac matrix and *det(D)* is the fermion determinant.

Since a Dirac fermion can be formed out of Majorana fermions, a slightly different result can be obtained for the Majorana case:

$$\int D\psi D\bar{\psi}e^{-\int d^4x\,\bar{\psi}(x)D\psi(x)}=det(D)=\prod_{j=1}^{2}\int d\lambda^j e^{-\int d^4x\frac{1}{2}\bar{\lambda}^j(x)D\lambda^j(x)} \tag{70}$$

$$\Rightarrow\int d\lambda\, e^{-\int d^4x\frac{1}{2}\bar{\lambda}(x)D\lambda(x)}=\pm\sqrt{det(D)} \tag{71}$$

The square root of the determinant as in (71) is also called the Pfaffian (*Pf*) (a phase factor can also be involved). The sign of the Pfaffian is undetermined in (71). To fix it, the following definition of the path integral is used:

$$\int d\lambda\, e^{-\int d^4x \frac{1}{2}\bar{\lambda}(x)D\lambda(x)} = \int d\lambda\, e^{-\int d^4x \frac{1}{2}\lambda(x)Q\lambda(x)} = Pf(Q) \tag{72}$$

where

$$Q = CD = -Q^T \tag{73}$$

C being the charge conjugation matrix. The Dirac matrix in the theory considered in this work is "γ_5-Hermitian", which means:

$$D^\dagger = \gamma_5 D\gamma_5 \Leftrightarrow \gamma_5 D = D^\dagger \gamma_5 \tag{74}$$

This implies that *det(D)* is a real quantity.

Further, *det(D)* is also non-negative, because:

$$CDC^{-1} = D^T \tag{75}$$

(in the theory under consideration).

Therefore, since *det(D)=det(Q)=|Pf(Q)|²*, *Pf(Q)* must be real, but can have any sign.

For several fermion actions, the Dirac matrix *D* can be formulated such that *det(D)* is positive. If it is not, what is done in practice is the replacement of *D* by *D†D*.

Then, for example, a generating functional becomes:

$$Z = \int DU\, D\lambda\, e^{-S_{gauge} - \bar{\lambda}D\lambda} = \int DU\, e^{-S_{gauge}} sign(Pf(Q))(det(D))^{\frac{1}{2}}$$

$$\Rightarrow Z = \int DU\, e^{-S_{gauge}} sign(Pf(Q))(det(D^\dagger D))^{\frac{1}{4}} \tag{76}$$

or

$$Z = \int DU\, e^{-S_{gauge}} sign(Pf(Q))(det(M))^{\frac{1}{4}}$$

with *M=D†D=M†* being a positive, Hermitian matrix. The determinant of *D* (or *M*) is to be calculated, and as mentioned before, this is not tractable via brute force because of the size and sparseness of the matrix. To circumvent this, the determinant is calculated using "pseudofermionic" variables (which are actually bosonic variables). This method was first put forward by Fucito, Marinari, Parisi & Rebbi[30]. With this method, the generating functional in (76) becomes:

$$Z=\int DU\prod_{n=1}^{NPF} D\varphi_n^\dagger D\varphi_n e^{-S_{gauge}[U]-S_{PF}[U,\varphi]} sign\left(Pf\left(Q\right)\right)$$

$$\tag{77}$$

$$S_{PF}[U,\varphi]=\frac{1}{2}\sum_{n=1}^{NPF} \varphi_n^\dagger M^{\frac{-1}{4n}} \varphi_n$$

This method is used heavily in this work. The calculation of the matrix *M*, in this work, is done using the rational approximation[31], which is discussed in Section 4.2.

So far, there doesn't seem to be a problem with putting fermionic fields onto a lattice. Unfortunately, there is one lurking around. It becomes apparent if one considers, for example, the propagator for a free fermion with mass *m*. The action to be considered is then the Dirac action, which, on the lattice is:

$$S_F=\frac{1}{2}\sum_x\sum_\mu \bar{\psi}(x)(\gamma_\mu\Delta_\mu+m)\psi(x)+h.c. \tag{78}$$

Δ_μ is the difference operator that replaces the continuum derivative. Calculating the propagator gives:

$$S^{-1}(p)=m_q+\frac{i}{a}\sum_\mu \gamma_\mu \sin(p_\mu a) \tag{79}$$

Because of the finite lattice spacing, the momenta are restricted to a Brillouin zone, taken to be {-π/a, π/a}. The zeros then lie at $p_\mu=0$ and π. Using these zeros of the four-momentum, define the sixteen possible four-vectors $\Pi^A=\{(0,0,0,0),(\pi,0,0,0)...(\pi,\pi,\pi,\pi)\}$ with $A=\{1,2...16\}$. Performing an expansion of the propagator in the massless limit around these zero points:

$$S^{-1}(p,m=0)=\frac{i}{a}\sum_\mu \gamma_\mu \sin(p_\mu a)=\frac{i}{a}\sum_\mu \gamma_\mu \sin((\Pi^A+k)_\mu a)$$

$$\tag{80}$$

$$\Rightarrow S^{-1}(p,m=0)=\frac{i}{a}\sum_\mu \gamma_\mu Sgn_\mu^A \sin(k_\mu a)$$

where Sgn_μ^A is ±1 depending on whether the μth component of Π^A is 0 or π. Taking the continuum limit $a\to 0$ for each of the 16 possibilities recovers the correct continuum form of the propagator, i.e. if any component of the momentum nears the limits of the Brillouin zone, the discretized fermion behaves like a fermion in the continuum. This leads to 2^d "tastes" (named as an analogy to particle flavor) of a fermion, which means that there is a doubling for every dimension. This is called "fermion doubling" and is one of the biggest issues to be solved when studying lattice theories.

21

There have been many formulations of fermions that remove the doubling problem. The formulation used in this work is that of Wilson. In this formulation, the 15 spurious doublers acquire a large mass at the edges of the Brillouin zone and disappear from the spectrum. The Wilson operator looks like:

$$(D_W)_{xy} = (m_0 + dr) \delta_{xy} - \frac{1}{2} \sum_\mu \left[(r - \gamma_\mu) U_\mu(x) \delta_{x+\mu,y} + (r + \gamma_\mu) U_\mu(x - \hat{\mu}) \delta_{x-\mu,y} \right] \tag{81}$$

m_0 is the bare mass of the fermion, d is the number of space-time dimensions considered and r is the Wilson parameter such that $0 < r \leq 1$. Casting the operator in another form allows for a clearer interpretation:

$$(D_W)_{xy} = \delta_{xy} - \kappa \sum_\mu \left[(r - \gamma_\mu) U_\mu(x) \delta_{x+\mu,y} + (r + \gamma_\mu) U_\mu(x - \hat{\mu}) \delta_{x-\mu,y} \right]$$

$$\kappa = \frac{1}{2(m_0 + dr)} \tag{82}$$

The effect of the first term, which is local, is to keep the fermion at the same lattice site. The other, non-local term makes the fermion "hop" to the neighboring site with a strength κ, leading to the nomenclature of κ as the "hopping parameter". During this "hop", the fermion acquires a rotation by $(r-\gamma_\mu)$ in spin space and by U_μ in color space.

The main disadvantage of this formulation is that chiral symmetry is broken even for vanishing m_0 when $r \neq 0$. In the case of SYM, SUSY is also broken. However, a tuning of the gaugino mass is enough to restore chiral symmetry (shown by Bochicchio, Maiani, Martinelli, Rossi & Testa)[32] as well as SUSY (shown by Curci & Veneziano)[33] in the continuum limit.

A sign problem of the Pfaffian exists, as shown by the DESY-Münster collaboration[34]. This is a potential roadblock to performing simulations effectively. If the frequency of the fluctuation of the sign is high, cancellations can occur, leading to an increase in statistical error. However, further investigation by the collaboration has shown that below a critical value of the hopping parameter (which is also the value of zero gaugino mass), negative Pfaffians do not occur[35–37]. As mentioned above, since SUSY is expected to be recovered in the limit of vanishing gaugino mass, one can avoid negative Pfaffians by taking this limit. There should then be no problems in performing Monte Carlo simulations of SYM with Wilson fermions.

22

3.5. Sources and mitigation of errors on the lattice

3.5.1. Sources (and possible reduction methods) of error

The results obtained using Monte Carlo simulations on the lattice will be different from physical results due to many sources of error. The most important contributions (in this work) come from:

• Statistical errors: The path integral formulation essentially takes into consideration all possible paths between two points and assigns different weights to them depending on the value of the action along the path. Generating an infinite number of such configurations on the computer is, of course, not possible. The finite number of configurations that are used in Monte Carlo calculations thus introduce an error, which is proportional to $1/n^{1/2}$, n being the number of configurations used. Hence, the more configurations one uses, the closer the approximation is to the continuum and the less the error.

• Finite lattice spacing: Since a discretization of space-time is non-physical, it should be evident that the lattice formulation will intrinsically introduce errors. The size of the errors depend on how closely the lattice operators approximate continuum behavior. The easily way to reduce these errors is thus to improve lattice actions (if possible), extract observables at a range of values of the lattice spacing a and then extrapolate to $a \rightarrow 0$. The Wilson formulation that is used in this work introduces errors of $O(a)$.

• Finite volume effects: This error arises due to the approximation of an essentially infinite system by a finite volume. The error is usually proportional to e^{-mL} [38] or a power law in L, such as $1/L^3$ [39]. The errors can be reduced, in principle, by increasing the size of the (side of the) lattice, L, but this increases computational load.

3.5.2. Estimating the errors

The statistical error introduced due to the finite number of configurations is estimated in this work using the Jackknife technique. It was first thought of by Quenouille[40] and extended by Tukey[41]. The average of the observable in question, *<O>*, is first calculated over the entire data set. The data is then divided into *M* blocks. One should take care to make the length of the blocks greater than the auto-

correlation time for the method to be effective. Each block is then removed from the data set and the average of the observable calculated using this reduced set. This average is denoted by $<O>_i$ with $i=1...M$. The error is estimated by calculating the deviation of these "jackknifed" averages from the average over the complete set:

$$\sigma = \sqrt{\frac{M-1}{M} \sum_{i=1}^{M} \left(\langle O \rangle_i - \langle O \rangle \right)^2} \tag{83}$$

The reason the technique works is because each jackknifed average contains almost the full set of data and so, is approximately equal to the full data set value.

4. Monte Carlo methods and algorithmic aspects

In order to compute observables in lattice theories, supersymmetric or not, an enormous number of integrations have to be performed. For example, consider (64). Even on a 2-dimensional 8x8 lattice with gauge group $SU(2)$, which parametrizes each link variable by 4 parameters, this number is in the thousands. If a grid of, say, 10 points per integration is used, the multiple integral will be approximated by a sum consisting of 10^{1000} terms on the conservative side. This makes a direct computation unfeasible. As noted earlier, however, lattice theories bear a striking resemblance to statistical models, from which it is known that out of all possible configuration, only a small subset effectively contribute to averages. Hence, an effective way of computing averages on the lattice would be to stochastically generate series of link variable configurations with a probability distribution given by the Boltzmann factor e^{-S}. The average will then be given by the mean value of several such configurations:

$$\langle O \rangle = \frac{1}{N} \sum_{i=1}^{N} O([U]_i) \tag{84}$$

The general requirement of an algorithm for generating such series of configurations is that it the configurations should eventually reach the desired probability distribution, at which point the system is said to be "thermalized". The thermalized configurations can then be used to measure an observable. Although the number of configurations that can be generated will always be finite, if the sequence generated by the algorithm constitutes a representative set, then the approximation given by the above equation will be good. There is a probability that each configuration can transit to another, determined by a transition matrix, as required by stochastic processes, such that:

$$P(C \rightarrow C') \geq 0$$

$$\sum_{C'} P(C \rightarrow C') = 1 \tag{85}$$

where C and C' denote configurations in general. The customary process is to change one particular variable at a time, proceeding through the lattice, then varying another, and so on until all variables have been sampled. This constitutes a Monte Carlo sweep of the lattice. However, a simultaneous variation of multiple variables can also be done.

A sufficient condition that must be satisfied so that an algorithm can generate configurations

with a probability of the Boltzmann factor is that each "step" of the transition matrix must satisfy detailed balance, i.e.:

$$e^{-S(C)}P(C \rightarrow C') = e^{-S(C')}P(C' \rightarrow C) \tag{86}$$

The detailed balance equation does not place any restrictions on the probability function that is used. This grants a level of freedom that can be used to implement new algorithms or constantly improve established ones based on the problem being investigated.

One of the earliest and simplest algorithms that can generate chains of configurations and satisfy detailed balance is the so-called Metropolis-Hastings algorithm. It is perhaps instructive to go through it, as it provides a general idea of how such algorithms work. The steps involved here are:

• A new configuration is selected based on an arbitrary probability function, the only requirement of which is:

$$P_0(C \rightarrow C') = P_0(C' \rightarrow C) \tag{87}$$

• The change in the action due to this change is calculated. If $\Delta S \leq 0$ (the action has been reduced), the new configuration is accepted.

• If not, a random number r is selected from the interval [0,1] with a uniform probability distribution. If $r \leq e^{-\Delta S}$, the change is accepted. If not, the new configuration is rejected and the process is repeated.

Although the classical configuration corresponds to the minima of the action, this conditional acceptance allows the system to increase its action and move away from classical configurations. The algorithm thus incorporates quantum fluctuations. One of the biggest benefits of the Metropolis-Hastings algorithm is that it is free of systematic errors. There are a couple of problems with it, however. Consider how one could pick the new configuration to be tested. The new configuration could be completely random. Although it will then be uncorrelated to the old one, it is very likely that such a change will induce a large change in the action, leading to very low acceptance rates. The system will then move very slowly through its configuration space. One could also choose $C' = C + \delta C$ and then tune δC so that ΔS is small, but this will introduce large correlations between successive configurations. If the computation of ΔS is expensive, as it is with supersymmetric lattice theories, neither of these

26

options are good ones. The other problem is with the scope of variables that are changed. The Metropolis-Hastings algorithm works best if a single variable is changed in each step. Changing multiple variables again leads to large ΔS and low acceptance rates. In fact, this problem also arises for single variable changes in actions depending non-locally on the co-ordinates. What is desired is then an algorithm that performs global updation and also has a high acceptance rate.

4.1. The Hybrid Monte Carlo (HMC) algorithm

The HMC algorithm combines molecular dynamics methods, which have high acceptance rates, with the Metropolis acceptance test. The result is an algorithm capable of globally updating variables, with a high acceptance rate and free of systematic errors. It was developed, in its complete form, by Duane, Kennedy, Pendleton & Roweth[42]. An outline of the steps involved is:

- A set of momenta $\{\pi_i\}$, conjugate to the co-ordinates $\{\varphi_i\}$, is chosen from a Gaussian ensemble:

$$P(\{\pi_i\})=(\prod_i \frac{1}{\sqrt{2\pi}})e^{-\sum_i \frac{\pi_i^2}{2}} \tag{88}$$

- A half step is performed:

$$\tilde{\pi}_i(n)=\pi_i(n)-\frac{\epsilon}{2}\frac{\partial S[\varphi]}{\partial \varphi_i(n)} \tag{89}$$

where n denotes a particular time step and ϵ is the value of a single time step.

- The following two equations are then iterated for a number of time steps, at the discretion of the user:

$$\varphi_i(n+1)=\varphi_i(n)+\epsilon\tilde{\pi}_i(n)$$

$$\tilde{\pi}_i(n+1)=\tilde{\pi}_i(n)-\epsilon\frac{\partial S[\varphi]}{\partial \varphi_i(n+1)} \tag{90}$$

- If $\{\varphi',\pi'\}$ and $\{\varphi,\pi\}$ denote the configurations after and before the iteration, the new configuration is accepted with probability:

$$P = min\left(1, e^{-H[\varphi', \pi']}/e^{-H[\varphi, \pi]}\right) \tag{91}$$

where H is the Hamiltonian of the system.

- If there is no acceptance, start over with the old configuration $\{\varphi, \pi\}$. If the new configuration is accepted, use the new co-ordinates and repeat the process from the second step onwards.

A few improvements to the above algorithm are implemented in this work, particularly higher order integrals and multiple time scales.

4.2. The rational Hybrid Monte Carlo (rHMC) algorithm

The pseudofermion method, as seen in (77), requires the calculation of the inverse of the fermion matrix. This is done using the rHMC algorithm, which was put forward by Horváth, Kennedy & Sint[31]. In this method, the term M^{-q}, where $q=1/4n$, is approximated rationally using:

$$r(x) = x^{-q} \approx \alpha_0 + \sum_{r=1}^{N_R} \frac{\alpha_r}{x + \beta_r} \tag{92}$$

The co-efficients α & β are calculated using the Remez algorithm[43]. The accuracy of the approximation depends mainly on the number of terms N_R used in the polynomial and the accuracy in the determination of α & β. In this work, N_R is 20 for the 8x8 lattice and 25 for the larger lattices in the interval $\{10^{-4}, 10\}$. The inversion of the fermion matrix using the rHMC approximation is then done using the Conjugate Gradient (CG) solver[44].

5. *N=2* SYM in 2D on the lattice

5.1. Dimensional reduction of 4-dimensional *N=1* SYM

The starting point is (35), the equation of an *N*=1 supersymmetric Yang-Mills theory in 4-dimensional Minkowski space-time. The idea is to assume that 2 of the space-time dimensions (here, x^2 & x^3) are compact and interpret them as internal degrees of freedom[45]. Fields no longer depend on these compactified dimensions and all derivatives with respect to these dimensions can be set to zero. In the following, *m* and *n* are used to denote all four dimensions, so *m,n*=1,2,3,4. Greek indices denote purely space-time indices, so, for example, μ=0,1 in 2 dimensions. The compactified dimensions are represented (directly or indirectly) using Latin indices, so, for example, *a*=2,3.

First, the Clifford algebra is defined in 2 and 4 dimensions. Let the gamma matrices in 2D be denoted by γ^μ and those in 4D by Γ^m. A representation of the 4D matrices is chosen to clearly see their construction from their 2D counterparts:

$$\Gamma^\mu = I_{2x2} \otimes \gamma^\mu \qquad \mu=0,1$$

$$\Gamma^{1+a} = \gamma_3 \otimes i\sigma_a \qquad a=1,2$$

(93)

I_{2x2} is the 2x2 identity matrix. The following representation of the 2D gamma matrices can be chosen[46]:

$$\gamma^0 = \begin{pmatrix} 1 & 0 \\ 0 & -1 \end{pmatrix} \qquad \gamma^1 = \begin{pmatrix} 0 & 1 \\ -1 & 0 \end{pmatrix} \qquad \gamma_3 = \gamma^0\gamma^1 = \begin{pmatrix} 0 & 1 \\ 1 & 0 \end{pmatrix}$$

(94)

Consider the pure Yang-Mills term. To maintain dimensionality in 2D, the gauge field components are re-scaled:

$$A_\mu \rightarrow \frac{A_\mu}{\sqrt{V_2}} \qquad \mu=0,1$$

$$\varphi_a \rightarrow \frac{\varphi_a}{\sqrt{V_2}} \qquad a=1,2$$

(95)

The φ_as are the (now scalar) components of the gauge field in the compactified dimensions. With this, the field strength becomes:

$$F_{\mu\nu}^{4D}=\partial_\mu\frac{A_\nu^{2D}}{\sqrt{V_2}}-\partial_\nu\frac{A_\mu^{2D}}{\sqrt{V_2}}-\frac{ig_{4D}}{V_2}[A_\mu^{2D},A_\nu^{2D}]=\frac{1}{\sqrt{V_2}}\left\{\partial_\mu A_\nu^{2D}-\partial_\nu A_\mu^{2D}-ig_{2D}[A_\mu^{2D},A_\nu^{2D}]\right\}$$

$$=\frac{F_{\mu\nu}^{2D}}{\sqrt{V_2}}$$

$$F_{\mu,1+a}^{4D}=\partial_\mu\frac{\varphi_a^{2D}}{\sqrt{V_2}}-\frac{ig_{4D}}{V_2}[A_\mu^{2D},\varphi_a]=\frac{1}{\sqrt{V_2}}\left\{\partial_\mu\varphi_a^{2D}-ig_{2D}[A_\mu^{2D},\varphi_a]\right\}=\frac{1}{\sqrt{V_2}}D_\mu^{2D}\varphi_a$$

$$F_{1+a,1+b}^{4D}=\frac{-ig_{4D}}{V_2}[\varphi_a,\varphi_b]=\frac{-ig_{2D}}{\sqrt{V_2}}[\varphi_a,\varphi_b]$$

(96)

where

$$g_{2D}=\frac{g_{4D}}{\sqrt{V_2}}$$

(97)

is the rescaled coupling constant in 2D. Substituting the above terms into the pure Yang-Mills term in the action and integrating over the compactified dimensions (which cancels all the V_2 co-efficients in the denominators), the dimensionally reduced Yang-Mills term is obtained:

$$S_{YM}=-\frac{1}{4}\int d^4x\,Tr\left(F^{mn}F_{mn}\right)\rightarrow-\frac{1}{4}\int d^2x\,Tr\left(F^{\mu\nu}F_{\mu\nu}+2D^\mu\varphi^a D_\mu\varphi_a-g_{2D}^2[\varphi^a,\varphi^b][\varphi_a,\varphi_b]\right)$$

(98)

The factor of 2 in the second term arises because $F^{\mu,1+a}F_{\mu,1+a}=F^{1+a,\mu}F_{1+a,\mu}$.

For the purpose of dimensionally reducing the Dirac term, the Majorana spinor is decomposed:

$$\lambda=\frac{1}{\sqrt{V_2}}\sum_{r=1}^{2}e_r\otimes\chi_r$$

(99)

e_r is a basis vector in 2D space-time and χ_r, with this normalization, is a Majorana spinor in 2D space-time. Similarly:

$$\bar\lambda=\lambda^\dagger\Gamma^0=\frac{1}{\sqrt{V_2}}\sum_{r=1}^{2}(e_r^T\otimes\chi_r^\dagger)(I_{2\times2}\otimes\gamma^0)=\frac{1}{\sqrt{V_2}}\sum_{r=1}^{2}e_r^T\otimes\chi_r^\dagger\gamma^0=\frac{1}{\sqrt{V_2}}\sum_{r=1}^{2}e_r^T\otimes\bar\chi_r$$

(100)

30

The covariant derivatives take the form:

$$D_\mu \lambda = \frac{1}{\sqrt{V_2}} \sum_{r=1}^{2} e_r \otimes D_\mu \chi_r$$

$$D_{1+a} \lambda = \frac{1}{\sqrt{V_2}} - i g_{2D} \sum_{r=1}^{2} e_r \otimes [\varphi_a, \chi_r] \tag{101}$$

Inserting these terms into the Dirac part of the action and integrating over the compactified dimensions:

$$\begin{aligned}
S_D &= \frac{i}{2} \int d^4 x Tr(\bar{\lambda} \Gamma^m D_m \lambda) \to \frac{i}{2} \int d^2 x Tr \Big[\sum_{rs} (e_r^T \otimes \bar{\chi}_r) \Gamma^m D_m (e_s \otimes \chi_s) \Big] \\
&= \frac{i}{2} \int d^2 x Tr \Big[\sum_{rs} (e_r^T \otimes \bar{\chi}_r)(e_s \otimes \gamma^\mu D_\mu \chi_s) - i g_{2D} \sum_{rs} (e_r^T \otimes \bar{\chi}_r)(\gamma_3 \otimes i \sigma_a)(e_s \otimes [\varphi_a, \chi_s]) \Big] \\
&= \frac{i}{2} \int d^2 x Tr \Big\{ \sum_{rs} (e_r^T e_s) \otimes (\bar{\chi}_r \gamma^\mu D_\mu \chi_s) - i g_{2D} \sum_{rs} [(e_r^T \gamma_3) \otimes (\bar{\chi}_r i \sigma_a)][e_s \otimes [\varphi_a, \chi_s]] \Big\} \\
&= \frac{i}{2} \int d^2 x Tr \Big[\sum_{rs} \delta_{rs} \otimes (\bar{\chi}_r \gamma^\mu D_\mu \chi_s) - i g_{2D} \sum_{rs} (e_r^T \gamma_3 e_s) \otimes (\bar{\chi}_r i \sigma_a [\varphi_a, \chi_s]) \Big] \\
&= \frac{i}{2} \int d^2 x Tr \Big[\sum_r (\bar{\chi}_r \gamma^\mu D_\mu \chi_r) - i g_{2D} \sum_{rs} (\gamma_3)_{rs} \otimes (\bar{\chi}_r i \sigma_a [\varphi_a, \chi_s]) \Big]
\end{aligned} \tag{102}$$

From the representation of γ_3 chosen, it can be seen that non-zero values exist only when $r \neq s$. Therefore, calling $i\sigma_a \equiv \gamma_a$:

$$\begin{aligned}
S_D &= \frac{i}{2} \int d^2 x Tr [\bar{\lambda} \gamma_\mu D_\mu \lambda - i g_{2D} (\bar{\chi}_1 \gamma_a [\varphi_a, \chi_2] - \bar{\chi}_2 \gamma_a [\varphi_a, \chi_1])] \\
&= \frac{i}{2} \int d^2 x Tr [\bar{\lambda} \gamma_\mu D_\mu \lambda - i g_{2D} (\bar{\chi}_1 \gamma_a \varphi_a \chi_2 - \bar{\chi}_1 \gamma_a \chi_2 \varphi_a + \bar{\chi}_2 \gamma_a \varphi_a \chi_1 - \bar{\chi}_2 \gamma_a \chi_1 \varphi_a)] \\
&= \frac{i}{2} \int d^2 x Tr [\bar{\lambda} \gamma_\mu D_\mu \lambda - i g_{2D} (\bar{\lambda} \gamma_a \varphi_a \lambda - \bar{\lambda} \gamma_a \lambda \varphi_a)] \\
&= \frac{i}{2} \int d^2 x Tr [\bar{\lambda} \gamma_\mu D_\mu \lambda - i g_{2D} \bar{\lambda} \gamma_a [\varphi_a, \lambda]]
\end{aligned} \tag{103}$$

Performing a further re-scaling of:

$$A_\mu \to \frac{1}{g_{2D}} A_\mu \qquad \varphi_a \to \frac{1}{g_{2D}} \varphi_a \qquad \lambda \to \frac{1}{g_{2D}} \lambda \tag{104}$$

the complete action can be written as:

$$S = \alpha \int d^2 x Tr \left(-\frac{1}{4} F^{\mu\nu} F_{\mu\nu} - \frac{1}{2} D^\mu \varphi^a D_\mu \varphi_a + \frac{1}{4} [\varphi^a, \varphi^b][\varphi_a, \varphi_b] + \frac{i}{2} \bar{\lambda} \gamma_\mu D_\mu \lambda + \frac{1}{2} \bar{\lambda} \gamma_a [\varphi_a, \lambda] \right) \tag{105}$$

where the factors of the coupling constant (and the "volume" V_2) have been absorbed by α, i.e.:

31

$$\alpha = \frac{V_{2D}}{g_{4D}^2} \tag{106}$$

The field content of the dimensionally reduced theory is a gauge field, two real scalar fields and a (four-component) Majorana fermion.

5.2. Wick rotation of the 2-dimensional theory

A Wick rotation is achieved by making the following substitutions:

$$\gamma_0 \to i\gamma_0 \qquad A_0 \to iA_0 \tag{107}$$

The Euclidean form of the action then reads:

$$S^E = \alpha \int d^2x \, Tr\left(\frac{1}{4} F_{\mu\nu} F_{\mu\nu} + \frac{1}{2} D_\mu \varphi_a D_\mu \varphi_a - \frac{1}{4}[\varphi_a, \varphi_b][\varphi_a, \varphi_b] + \frac{1}{2}\bar{\lambda}\,\gamma_\mu^E D_\mu \lambda - \frac{1}{2}\bar{\lambda}\,\gamma_a^E[\varphi_a, \lambda]\right) \tag{108}$$

5.3. The lattice form of the theory

For the sake of avoiding a cluttered presentation, let us split the total lattice action.

$$S_{lattice} = S_{boson} + S_{fermion}$$

$$where \quad S_{boson} = S_{gauge} + S_{scalar} \tag{109}$$

The form of the gauge part of the action that is used has already been mentioned: the Symanzik action, which is reproduced here:

$$S_{gauge} = S_{Symanzik} = \frac{5\beta}{3} \sum_{plaquette} \Re(Tr\, U_{plaquette}) - \frac{\beta}{12} \sum_{1x2\,rectangle} \Re(Tr\, U_{1x2rectangle}) \tag{110}$$

From the definitions of β (60) and α (106), one can see that the two are related and can convert between them according to convenience.

The scalar action has two contributions, the kinetic part and the potential (the commutator). The kinetic part reads:

$$S_{scalar}^{kinetic} = -[\varphi_1(x) U_\mu(x) \varphi_1(x+\hat{\mu}) + \varphi_2(x) U_\mu(x) \varphi_2(x+\hat{\mu})] + 2[\varphi_1(x)\varphi_1(x) + \varphi_2(x)\varphi_2(x)] \tag{111}$$

For the commutator term, we expand the scalar fields (which are in the adjoint representation) in terms of the generators and simplify:

$$
\begin{aligned}
S_{scalar}^{potential} &= Tr\left\{ -\frac{1}{4}[\varphi_i(x),\varphi_j(x)][\varphi_i(x),\varphi_j(x)] \right\} \\
&= Tr\left\{ -\frac{1}{4}[\varphi_i^a(x)T^a, \varphi_j^b(x)T^b][\varphi_i^c(x)T^c, \varphi_j^d(x)T^d] \right\} \\
&= Tr\left\{ -\frac{1}{4}\varphi_i^a(x)\varphi_j^b(x)[T^a,T^b]\varphi_i^c(x)\varphi_j^d(x)[T^c,T^d] \right\} \\
&= Tr\left\{ -\frac{1}{4}\varphi_i^a(x)\varphi_j^b(x)f^{abm}T^m \varphi_i^c(x)\varphi_j^d(x)f^{cdn}T^n \right\} \\
&= -\frac{1}{4}Tr(T^m T^n)f^{abm}f^{cdn}\varphi_i^a(x)\varphi_j^b(x)\varphi_i^c(x)\varphi_j^d(x) \\
&= -\frac{1}{4}\delta^{mn}f^{abm}f^{cdn}\varphi_i^a(x)\varphi_j^b(x)\varphi_i^c(x)\varphi_j^d(x) \\
&= -\frac{1}{4}f^{abn}f^{cdn}\varphi_i^a(x)\varphi_j^b(x)\varphi_i^c(x)\varphi_j^d(x) \\
&= -\frac{1}{4}f^{abcd}\varphi_i^a(x)\varphi_j^b(x)\varphi_i^c(x)\varphi_j^d(x)
\end{aligned}
\tag{112}
$$

where $f^{abcd} = f^{abm}f^{cdn}$ and the generators are normalized so that $Tr(T^aT^b) = \delta^{ab}$.

The lattice action for the fermions is written in the form:

$$S_{fermion} = \bar{\lambda} D_{lattice} \lambda \tag{113}$$

As with the scalars, there are two contributions to $D_{lattice}$, the kinetic term and the Yukawa potential term. The kinetic term on the lattice is the Wilson operator that was discussed earlier, so:

$$D_{lattice}^{kinetic} = (D_{Wilson})_{xy} = \delta_{xy} - \kappa \sum_\mu \left[(r - \gamma_\mu) U_\mu(x)\delta_{x+\mu, y} + (r + \gamma_\mu) U_\mu(x-\hat{\mu})\delta_{x-\mu, y} \right]$$

$$\kappa = \frac{1}{2(m_0 + 2r)} \tag{114}$$

The substitution of $d=2$ has been made for this particular theory. Using an expansion in the generators and proceeding as with the scalars, the Yukawa term on the lattice has the form:

$$D_{lattice}^{Yukawa} = -\gamma_a f^{mnp}\varphi_i^p(x) \tag{115}$$

where a sum over $i=1,2$ for the two scalars is to be done. Substituting (110), (111), (112) & (113) into (109) yields the action that is first used for the simulations.

33

6. Simulation results

For the simulations, the link variables have been taken to be unitary matrices from the group SU(2). As a preliminary step, simulations were first performed on an 8x8 lattice to find optimal values of α. To do this, the average plaquette was calculated for a range of α values. This was done because plaquette values of zero and one describe trivial and non-interacting theories. A well-tested range of the plaquette value is between 0.5-0.8 (for example, see [47]). A plot of the average plaquette versus α is shown in Fig. 6.1. (For the preliminary simulations, statistics of 500 configurations were used. For the main simulations, an 8x8 lattice with statistics of 5000 configurations and a 16x16 lattice with statistics of 1000 configurations were used.)
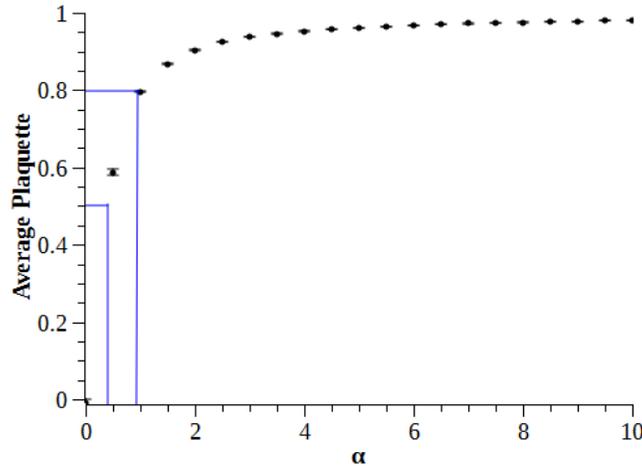
Fig. 6.1: Average plaquette as a function of the coupling α.

So, a plaquette range of 0.5-0.8 leaves an α range of ~0.4-0.9 available to us. In the main simulations, two values of α, 0.7 and 0.9, were chosen.

While performing these simulations, an instability of the theory was revealed. The potential term for the scalars has flat directions. The fields composing these directions can fluctuate to arbitrarily large values with no cost to the potential energy. This, in turn, causes the Hamiltonian to change drastically, leading to low acceptance rates and a breakdown of the simulation. This is shown in Fig. 6.2, where the scalar field is plotted as a function of the configuration number.

34
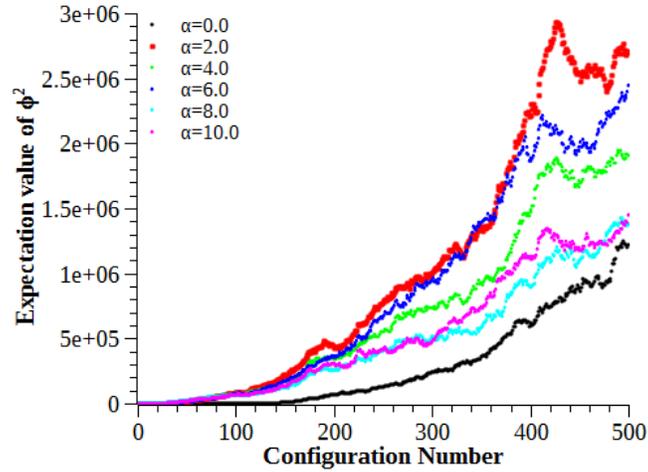
Fig. 6.2: $\langle\phi^2\rangle$ as a function of configuration number for five different values of α.

As one can see, the expectation value of the square of the scalar field increases rapidly to very large values with no sign of stabilization. To solve this problem, a mass term for the scalar fields was added.

6.1. The addition of the scalar mass term and stabilization of the theory

The term is specifically:

$$m_{scalar}\left(\varphi_1(x)\varphi_1(x)+\varphi_2(x)\varphi_2(x)\right) \tag{116}$$

This prevents the scalar field from blowing up, as shown in Fig. 6.3.
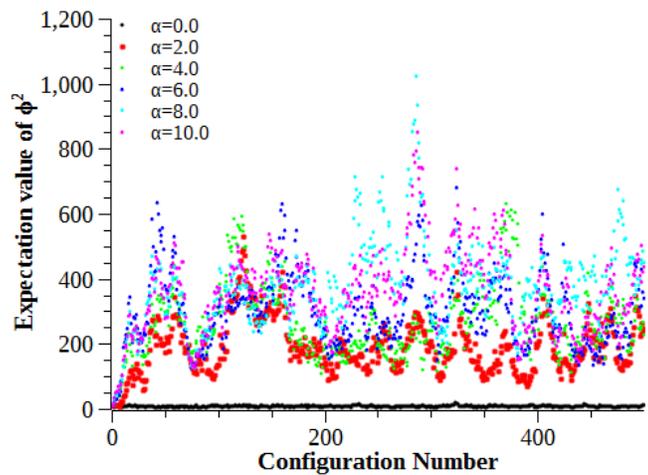
Fig. 6.3: $\langle\phi^2\rangle$ as a function of configuration number for different values of α after the addition of the mass term.

The expectation value of ϕ^2 stabilizes very quickly now and shows a constant dipping and rising about an average value.

6.2. Simulation parameters

With the addition of the mass term, there are now three parameters to consider:

- the coupling α, for the purpose of ultimately constructing the continuum limit. This is usually done by taking the limit $\alpha \to \infty$, since α is inversely related to the lattice spacing. As mentioned earlier, two values of α have been used in this work (from examining the plaquette values), 0.7 and 0.9.

- the bare gaugino mass, for the purpose of restoring supersymmetry. The bare mass is contained in the hopping parameter κ (see (82)). To repeat an earlier point, chiral symmetry and SUSY are broken on the lattice when the Wilson formulation of fermions is used. A tuning of the gaugino mass restores both. What observable signs does the symmetry breaking leave that we can use for the tuning? In SYM with gauge group $SU(N)$, the global discrete chiral symmetry Z_{2N} is broken spontaneously by a non-zero chiral condensate. A consequence of this is the expectation of the existence of a first-order phase transition at vanishing effective gaugino mass. A first order phase transition should also present with a double peak structure if a histogram of the chiral condensate is plotted. The value of the bare gaugino mass obtained using this method can be compared to the results from another test: although the gaugino is not part of the physical spectrum (due to confinement), in [48], using chiral perturbation theory and the OZI rule (from QCD), the renormalized gaugino mass has been related to the pion mass:

$$m_g \propto m_\pi^2 \tag{117}$$

Veneziano and Yankielowicz have argued[49] that the connected part of the η' meson is analogous to the pion. Thus, by measuring the square of the mass of the "pion" as a function of the bare gaugino mass, the value of the bare gaugino mass corresponding to zero effective gaugino mass can be extrapolated. The bare gaugino mass has been scanned between 0 and -1.

- the scalar mass. This has been added for stabilizing the theory, but it breaks SUSY in the process. The symmetry can be easily restored, however, by taking the limit $m_{scalar} \to 0$. Three values of the scalar

36

mass have been used: 0.002, 0.01 & 0.05.

6.3. The bosonic Ward identity

In order to investigate the restoration of supersymmetry on the lattice, the bosonic Ward identity, i.e. the expectation value of the bosonic action, was studied. This identity reads[50]:

$$\langle S_B \rangle = \frac{n-n_0}{2} \tag{118}$$

where n is the total number of bosonic (or equivalently, fermionic) degrees of freedom and n_0 is the number of zero modes. The total number of degrees of freedom

$$n = n_C n_S \tag{119}$$

where n_C is the number of colour degrees of freedom (=3) and n_S is the number of spinor degrees of freedom (=4). Therefore, $n=12$. The number of zero modes $n_0=n_C$, giving:

$$\langle S_B \rangle = \frac{12-3}{2} = 4.5 \tag{120}$$

This has been demonstrated in earlier studies[51] and it was satisfied here as well (without the mass term for the scalars, of course), as seen in Fig. 6.4.
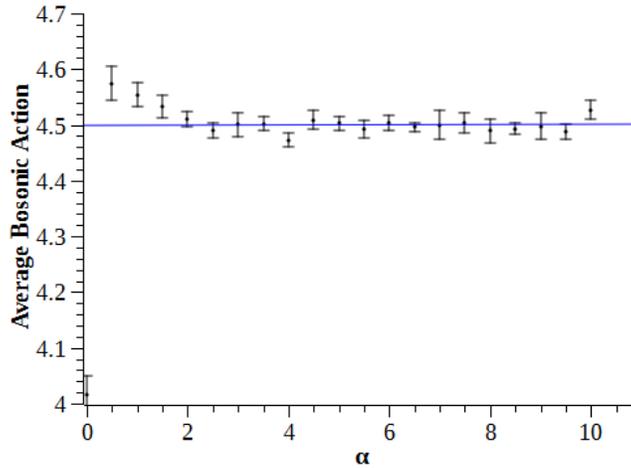
Fig. 6.4: The bosonic Ward identity as a function of α.

There are some deviations from the expected value for the lower values of α. For $\alpha=0$, the plaquette is also 0, representing a trivial theory and this causes the deviation of the first point. As α increases, the

average bosonic action rises to the expected value, but there are still deviations from the theoretical value. This is because the figure presented is for κ=0.277, which is not the critical value at which the effective gaugino mass vanishes, as will be seen a little later. However, for further increasing values of α (i.e. towards the continuum limit), the results agree, since the Ward identities should be fulfilled exactly in the continuum limit. It is expected that at the critical point of κ and in the continuum limit, the deviations will disappear.

The addition of the mass term changes the identity and the change can be calculated. The modification is essentially (for one of the scalar fields):

$$\left\langle m_{scalar}\varphi^2\right\rangle = \frac{\int D\varphi\, e^{-(S_B + m_{scalar}\varphi^2)}m\varphi^2}{\int D\varphi\, e^{-(S_B + m_{scalar}\varphi^2)}} \tag{121}$$

The fermionic part of the action need not be considered because it is only linear in φ. Looking in the flat directions of the potential, where the term $m_{scalar}\varphi^2$ plays a major role, the term S_B can be ignored, leading to:

$$\left\langle m_{scalar}\varphi^2\right\rangle = \frac{\int D\varphi\, e^{-m_{scalar}\varphi^2}m\varphi^2}{\int D\varphi\, e^{-m_{scalar}\varphi^2}} \tag{122}$$

With

$$Z = \int D\varphi\, e^{-m_{scalar}\varphi^2} = \sqrt{\frac{\pi}{m_{scalar}}} \tag{123}$$

(122) can be written as:

$$\begin{aligned}
\left\langle m_{scalar}\varphi^2\right\rangle &= -m_{scalar}\frac{\partial(\ln Z)}{\partial m_{scalar}}\\
&= -m_{scalar}\frac{1}{Z}\frac{\partial Z}{\partial m_{scalar}}\\
&= -m_{scalar}\sqrt{\frac{m_{scalar}}{\pi}}\frac{\partial}{\partial m_{scalar}}\left(\sqrt{\frac{\pi}{m_{scalar}}}\right)\\
&= \frac{1}{2}
\end{aligned} \tag{124}$$

Considering both scalar fields, this means the mass term should increase the Ward identity by 1. This is proven in figures 6.5 and 6.6, where the term $m_{scalar}\phi^2$ is plotted for both lattice sizes and all values of α and m_{scalar}. To show the behavior of this term as a function of HMC time, a few representative values of κ are used in figures 6.5 and 6.7. In figures 6.6 and 6.8, which plot the expectation value of $m_{scalar}\phi^2$,

three values of κ are used covering the entire scan range.
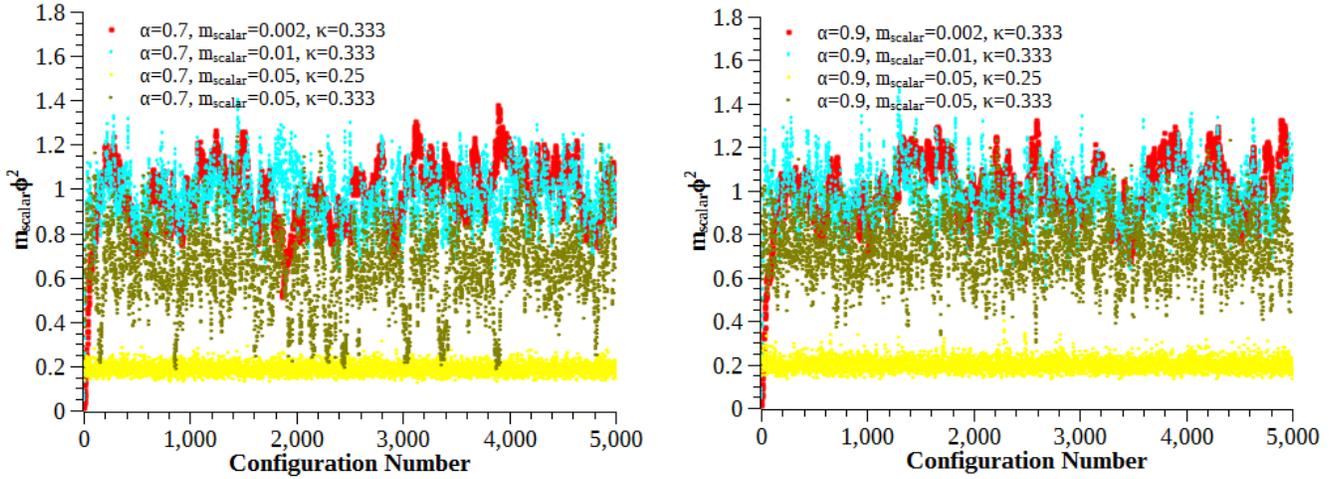
Fig. 6.5: The term $m_{scalar}\phi^2$ as a function of configuration number on the 8x8 lattice for α=0.7 (left) and α=0.9 (right). A scalar mass of 0.05 is revealed to be too heavy to retain supersymmetry.
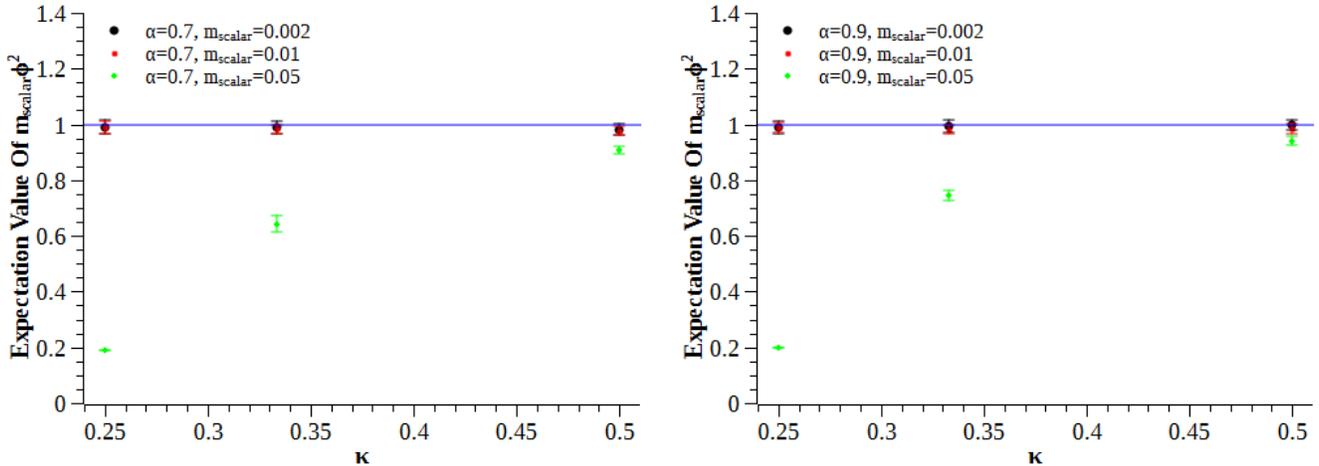
Fig. 6.6: $<m_{scalar}\phi^2>$ vs. κ on the 8x8 lattice for α=0.7 (left) and α=0.9 (right). The deviation from the theoretical values for a scalar mass of 0.05 is especially clear in these diagrams.

Scalar masses of 0.002 and 0.01 leave the increase of the bosonic action in very good agreement with the theoretical prediction. For a scalar mass of 0.05, large deviations occur. Although the increase in the bosonic action tends to 1 for increasing κ, such values are much larger than the critical value of κ, as will be seen later.
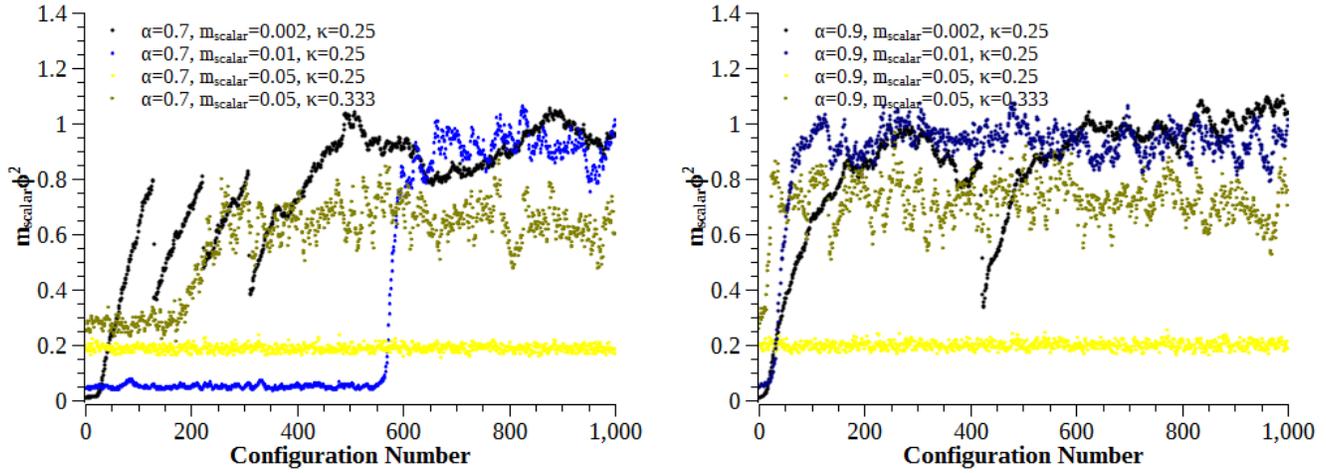
Fig. 6.7: The term $m_{scalar}\phi^2$ as a function of configuration number on the 16x16 lattice for α=0.7 (left) and α=0.9 (right). The problem with a scalar mass of 0.05 persists and some new anomalies are seen.
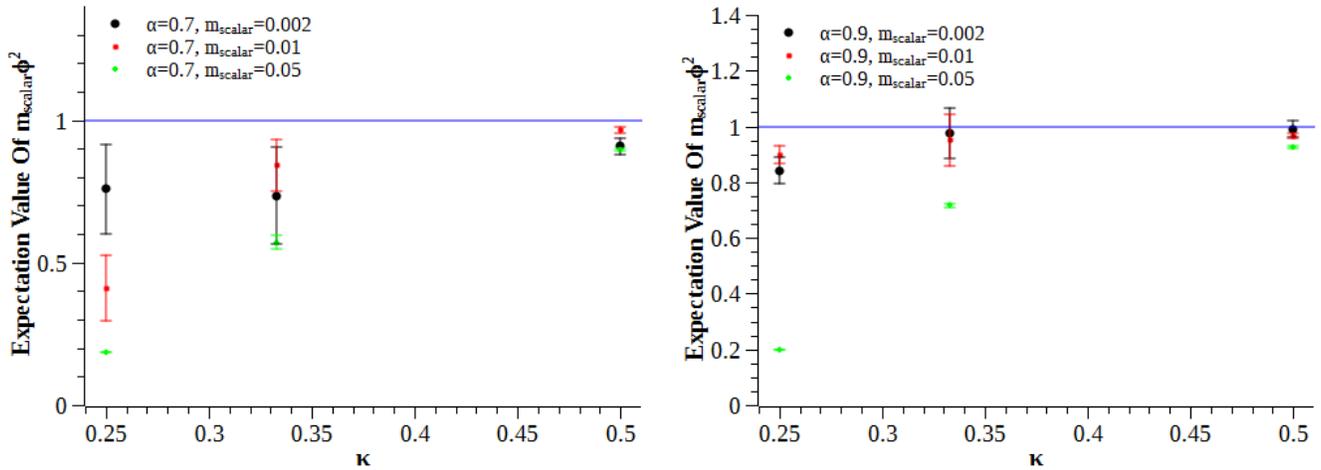
Fig. 6.8: $<m_{scalar}\phi^2>$ vs. κ on the 16x16 lattice for α=0.7 (left) and α=0.9 (right).

There are a few interesting points to note in the 16x16 lattice. In figure 6.7, for the lowest scalar mass, 0.002, for α=0.7, the increase in the bosonic action fluctuates multiple times for the first third of configurations and then appears to begin stabilization. This is a little better for α=0.9. Such fluctuations usually indicate problems with the change in the Hamiltonian and hence acceptance. This will be investigated in the next section. For a scalar mass of 0.01, a long thermalization time is also observed for α=0.7, which becomes much shorter for α=0.9. This is a shortcoming in the simulations performed. Optimally, a larger number of configurations is preferred, which always leads to better statistics.

On both the lattices, it is clearly seen that setting m_{scalar} to 0.05 results in deviations from the predicted increase of 1. This value is perhaps too high for the theory to remain supersymmetric.

6.4. The problem with m_{scalar}=0.002
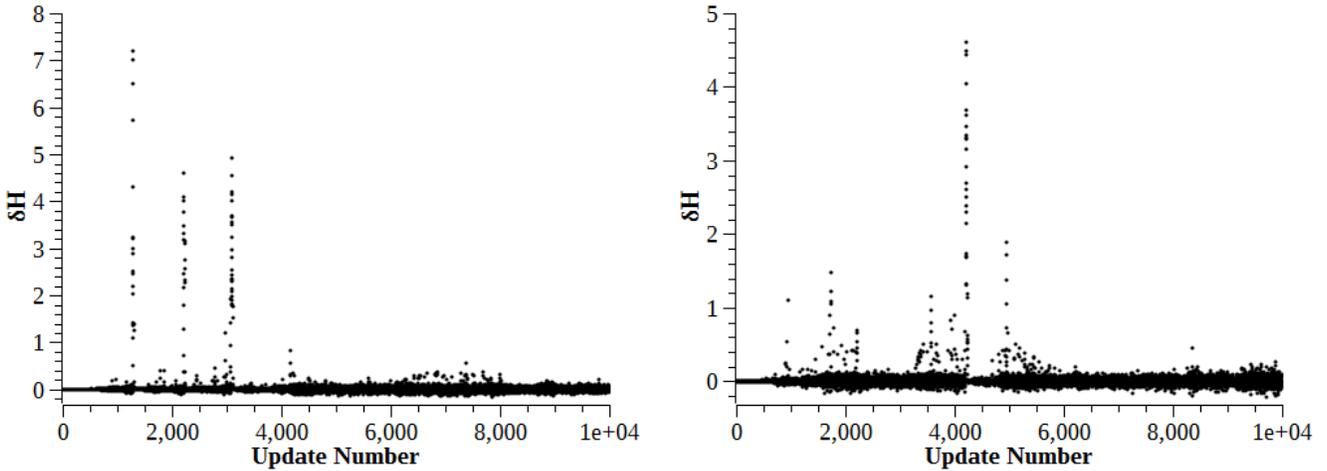
Fig. 6.9: δH plotted as a function of the update number for a scalar mass of 0.002 and α=0.7 (left) and α=0.9 (right).

There are indeed large changes in the Hamiltonian as was conjectured. This leads to large autocorrelation times. In figure 6.9, the change in the Hamiltonian is plotted as a function of the update number (there are 10 updates for every configuration). For this reason, this value of the scalar mass is also neglected for the principal results of this work.

6.5. The bosonic Ward identity, continued

With the inclusion of the scalar mass term, the average bosonic action should be around 5.5, which is shown in figures 6.10 and 6.11. The problem with m_{scalar}=0.05 is again apparent in these diagrams.
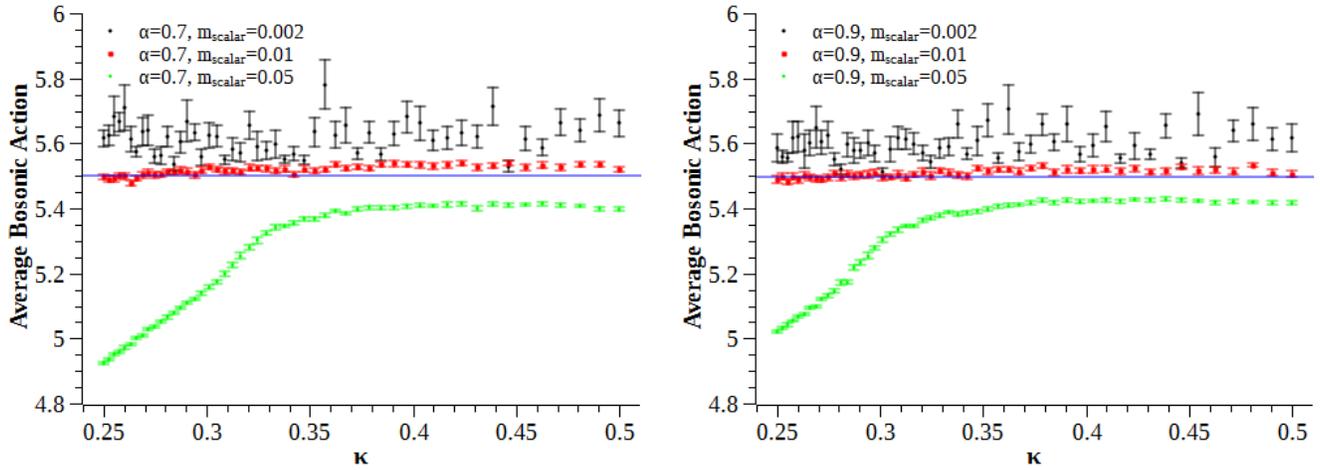
Fig. 6.10: The bosonic action density as a function of κ on the 8x8 lattice for α=0.7 (left) and α=0.9 (right).
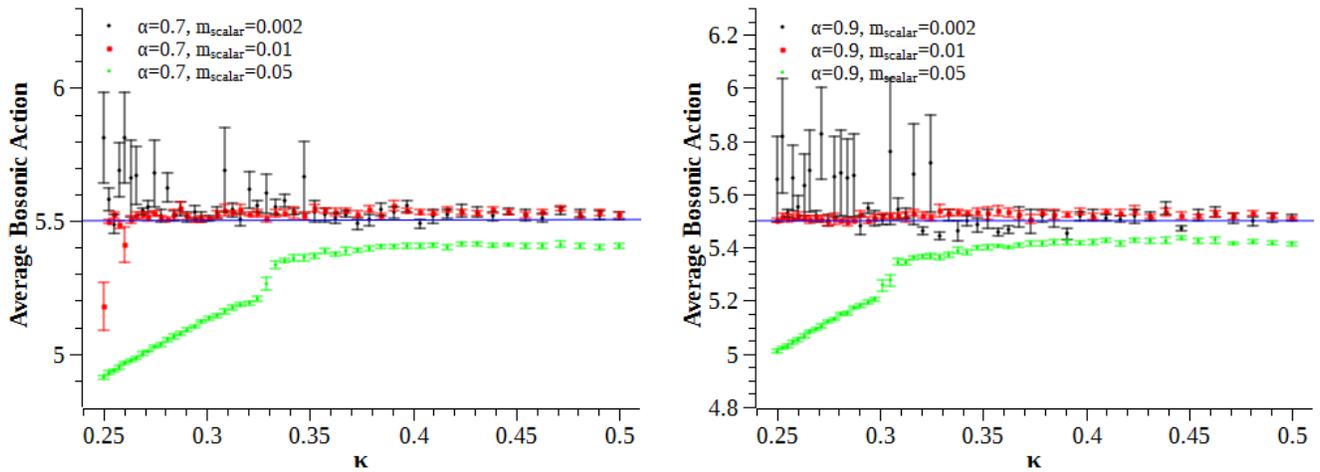
Fig. 6.11: The bosonic action density as a function of κ on the 16x16 lattice for α=0.7 (left) and α=0.9 (right).

The most obviously interesting thing first: for a scalar mass of 0.05, for both values of α, there seems to be a sudden jump in the value of the bosonic action, which may be an indicator of a first-order transition. It also looks like the Ward identity is satisfied for all values of κ (in the optimal case of m_{scalar}=0.01), which shouldn't be the case. The correct value of 5.5 should correspond to the critical value of κ. Figures 6.12 and 6.13 present the data for m_{scalar}=0.01 within a narrower range.
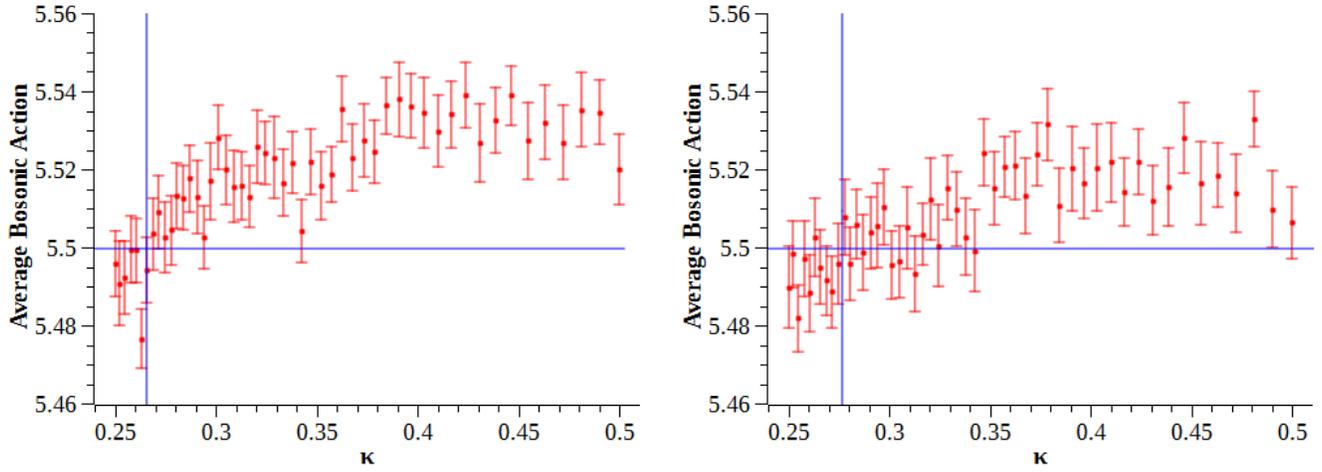
Fig. 6.12: A close-up of the bosonic action density vs. κ for m_{scalar}=0.01 on the 8x8 lattice and α=0.7 (left) and α=0.9 (right).
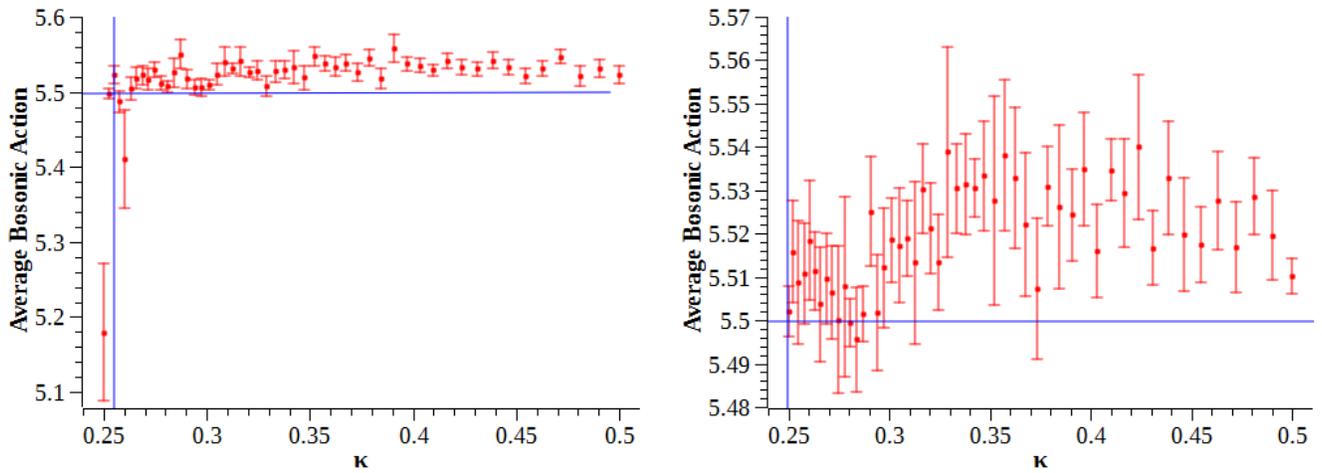
Fig. 6.13: A close-up of the bosonic action density vs. κ for m_{scalar}=0.01 on the 16x16 lattice and α=0.7 (left) and α=0.9 (right).

From figure 6.12, it is observed that the value of κ for which the action is 5.5 shifts to higher values as α increases, meaning it goes closer to the continuum limit. Unfortunately, the statistics used for the 16x16 lattice preclude the drawing of a meaningful conclusion. The shifting of the critical value of κ can be compared with the results of the next section, where the chiral condensate is examined.

6.6. The chiral condensate

The transition that the chiral condensate is expected to undergo at the critical point (where the

effective gaugino mass vanishes) is examined here. Figure 6.14 shows the chiral condensate for both values of α and on both lattice sizes for a scalar mass of 0.01 plotted as a function of the κ.
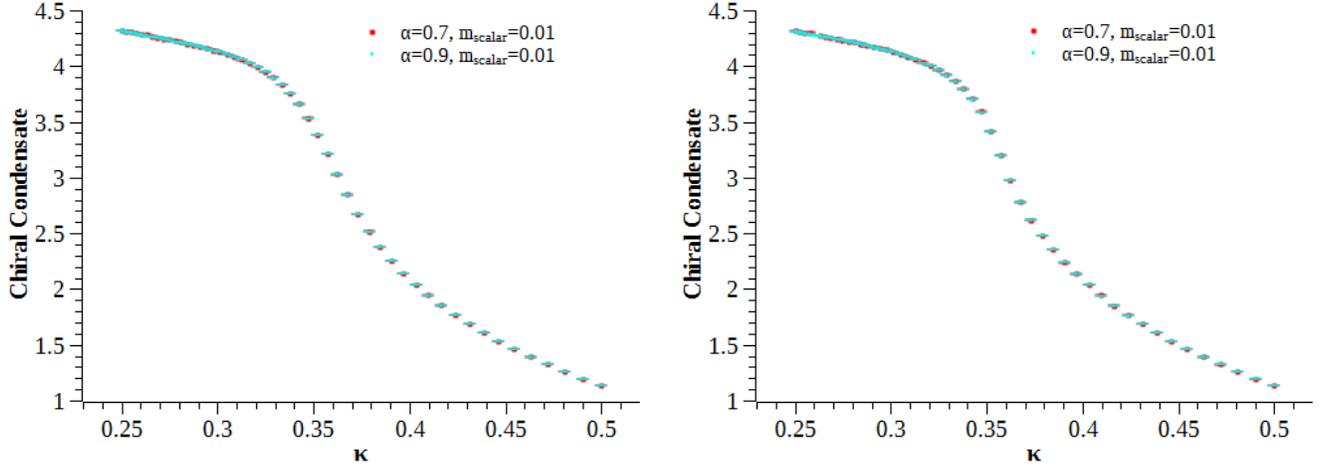

Fig. 6.14: The chiral condensate for α=0.7 and 0.9 and m_{scalar}=0.01 as a function of κ on the 8x8 lattice (left) and the 16x16 lattice (right).

The chiral condensate then underwent multiplicative and additive renormalization to compensate for the residual Wilson mass at finite lattice spacing. Assuming that the Wilson mass is a linear function of κ, since it is the gaugino mass, the following function was used[52]:

$$\Sigma_{ren}(\kappa) = Z_1 \Sigma(\kappa) - Z_2 \kappa - Z_3 \qquad (125)$$

The co-efficients Z_1, Z_2 & Z_3 were then fixed so that $\Sigma_{ren}(\kappa \ll \kappa_C)=1=-\Sigma_{ren}(\kappa \gg \kappa_C)$. The main idea is to make the chiral condensate a linear function of κ at values far from the critical values and then adjust the co-efficients so that they are approximately symmetrical about the zero value. This renormalized chiral condensate is shown in figure 6.15.
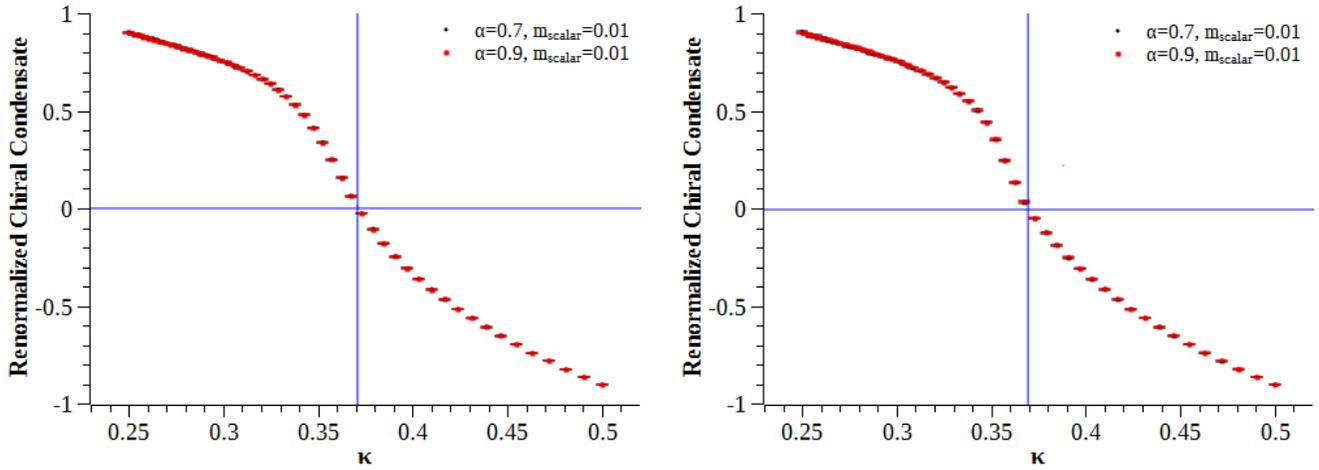
Fig. 6.15: The renormalized chiral condensate for α=0.7 and 0.9 and m_{scalar}=0.01 as a function of κ on the 8x8 lattice (left) and the 16x16 lattice (right).

The critical value of κ can then be extracted from the graphs and it is seen that:

$$\kappa_C(8\text{x}8)=0.3709(7) \quad \text{and} \quad \kappa_C(16\text{x}16)=0.3695(7)$$

The (renormalized) chiral condensate for a scalar mass of 0.05 showed some interesting characteristics, as seen in figure 6.16.
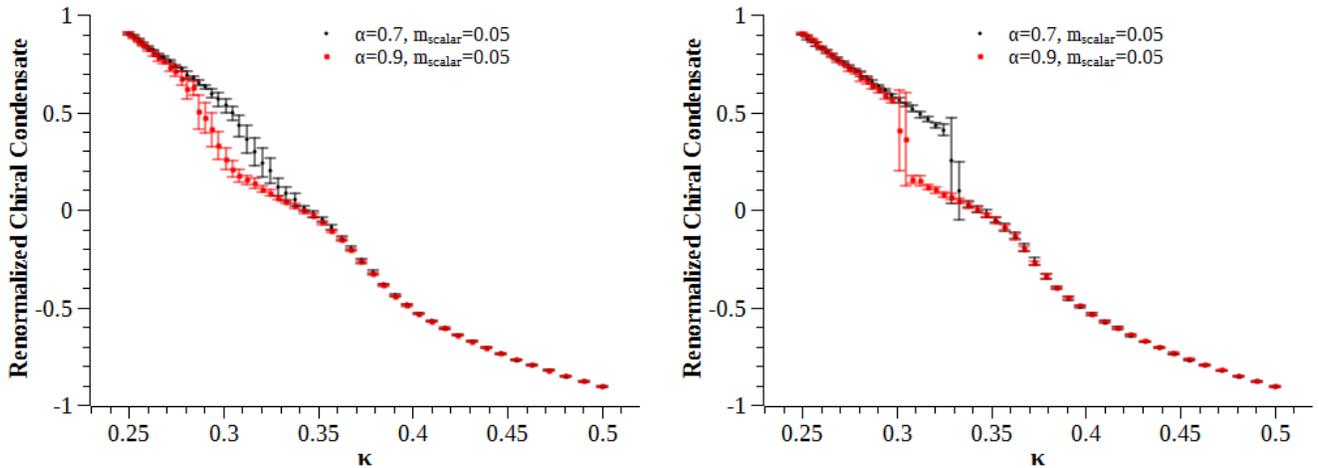
Fig. 6.16: The renormalized chiral condensate for α=0.7 and 0.9 as a function of κ on the 8x8 lattice (left) and the 16x16 lattice (right).

The chiral condensate displays what appears to be a hysteresis loop on both lattices, with the loop becoming larger and sharper for larger volume. If it is indeed a hysteresis loop, implies that a first-order

phase transition should take place in this region. A further investigation of this and its implications are discussed at length in section 6.8. It is also unclear whether there is another transition at higher values of κ, similar to the one observed for m_{scalar}=0.01, from which the critical value was just extracted. This will also be discussed later.

6.7. The (square of the) pion mass

Unfortunately, the square of the pion mass could not be calculated accurately on the 8x8 lattice, since a larger volume results in better statistics and comparatively reduced errors. Figure 6.17 shows the square of the pion mass as function of κ.
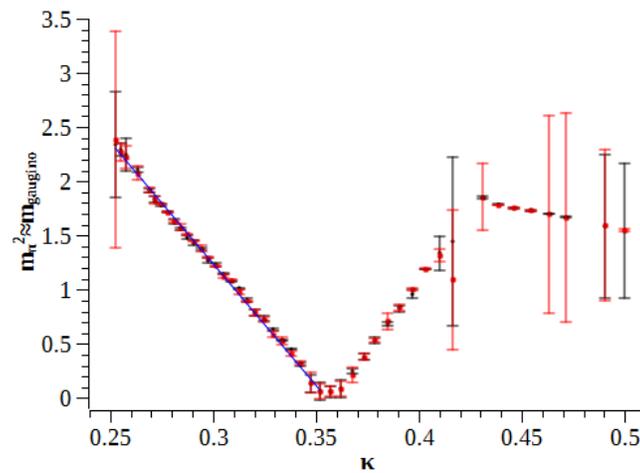
Fig. 6.17: The pion mass as a function of κ, for both values of α and a scalar mass of 0.01.

A linear fit to the data and extrapolation to zero κ delivers the critical value at which the effective gaugino mass vanishes:

$$\kappa_C=0.358(2)$$

This value is about 3.1% different from the value obtained using the chiral condensate transition, so the two values agree quite well.

6.8. m_{scalar}=0.05 and symmetry breaking

   In the previous sections, two indications of a first-order transition taking place for a scalar mass of 0.05 were seen: the sudden increase in the bosonic action in figure 6.11 and the loop seen in figure 6.16. In order to verify this, both the (square of the) scalar field and the chiral condensate may be plotted as a function of HMC time (i.e. as a function of the configuration number). It would then be reasonable to expect sharp changes in their values at the point of the transition. Since the jump and the loop are much clearer on the 16x16 lattice, this is the size used. Figure 6.18 shows the square of the scalar field as a function of HMC time for both values of α.
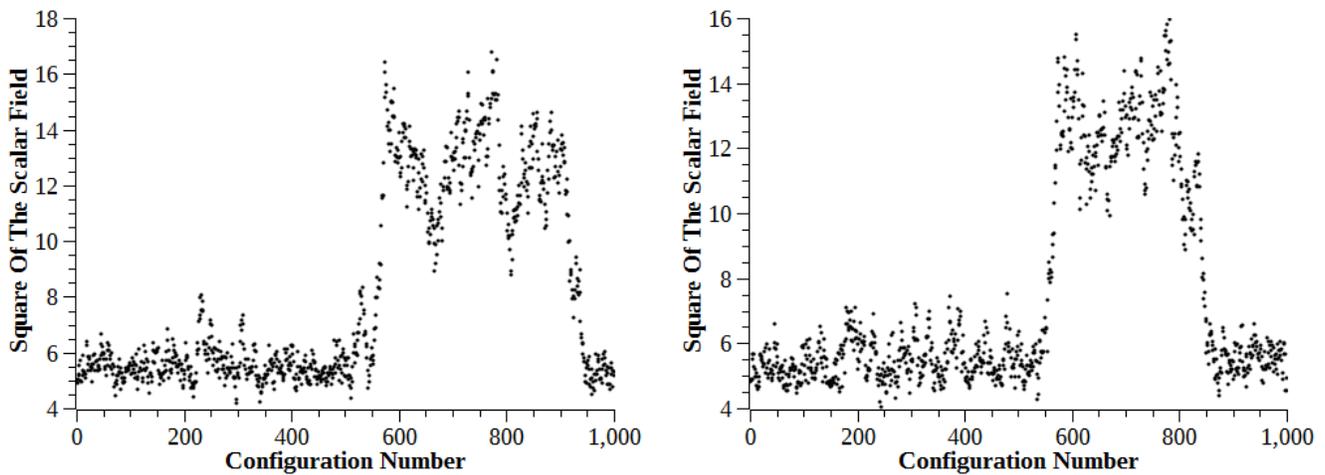
Fig. 6.18: The square of the scalar field as a function of configuration number for m_{scalar}=0.05 on the 16x16 lattice for α=0.7 and κ=0.328 (left) and α=0.9 and κ=0.301 (right).

The sharp transitions characteristic of a first-order phase transition are clearly visible. As one moves in either direction of this transition point, one would expect a clear separation of phases, i.e. the system should be only in one of the two phases. This is demonstrated in figure 6.19.

47
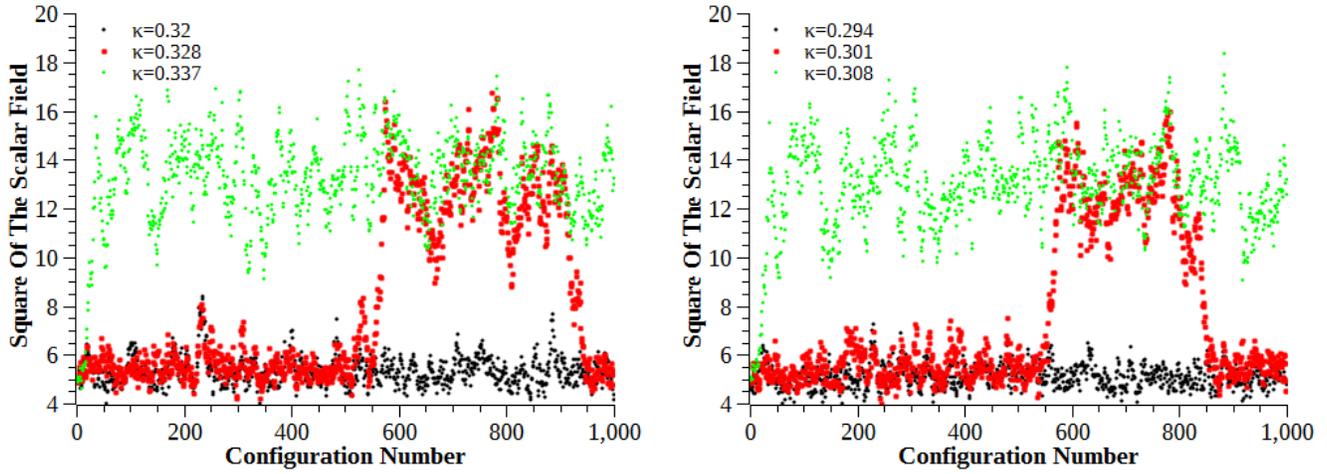
Fig. 6.19: The square of the scalar field as a function of configuration number for m_{scalar}=0.05 on the 16x16 lattice for α=0.7 & κ=0.32, 0.328 & 0.337 (left) and α=0.9 & κ=0.294, 0.301 & 0.308 (right).

This was repeated for the chiral condensate. The sharp change at the transition point is shown in figure 6.20 and the presence of two separate phases at gaugino masses away from the transition point in figure 6.21.
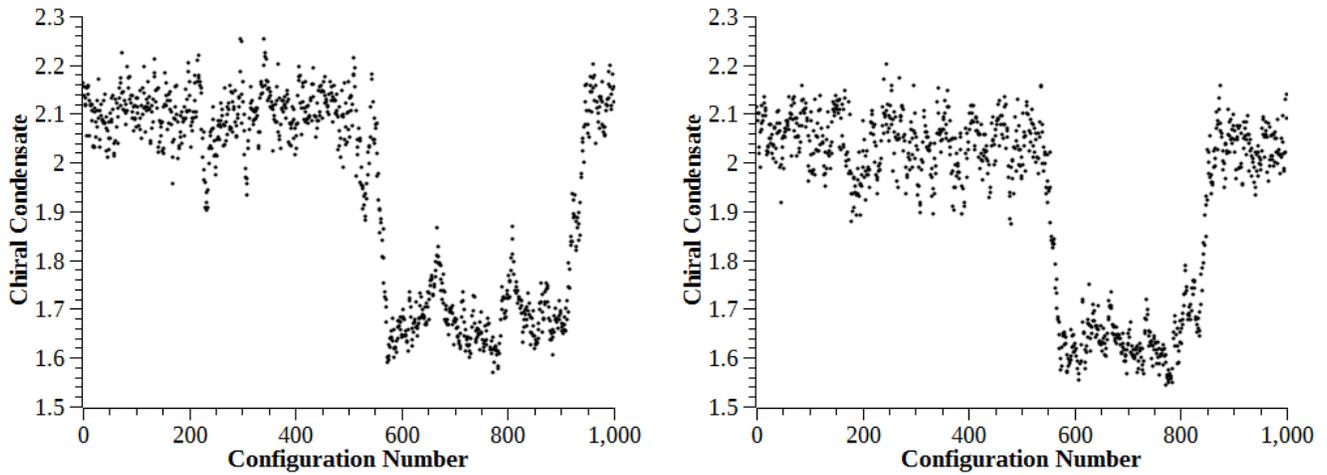

Fig. 6.20: The chiral condensate as a function of configuration number for m_{scalar}=0.05 on the 16x16 lattice for α=0.7 & κ=0.328 (left) and α=0.9 & κ=0.301 (right).
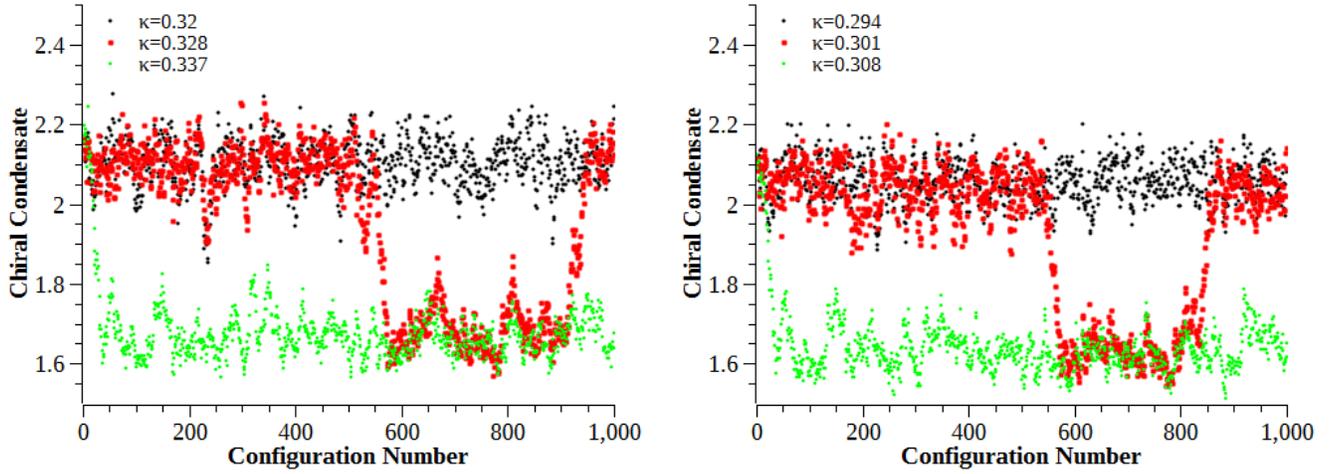
Fig. 6.21: The chiral condensate as a function of configuration number for m_{scalar}=0.05 on the 16x16 lattice for α=0.7 & κ=0.32, 0.328 & 0.337 (left) and α=0.9 & κ=0.294, 0.301 & 0.308 (right).

As was discussed in section 6.2, another indication of a first-order phase diagram is the presence of a double-peaked structure when a histogram of the chiral condensate is plotted. This is shown in figure 6.22 for the same two cases as considered in figure 6.20.
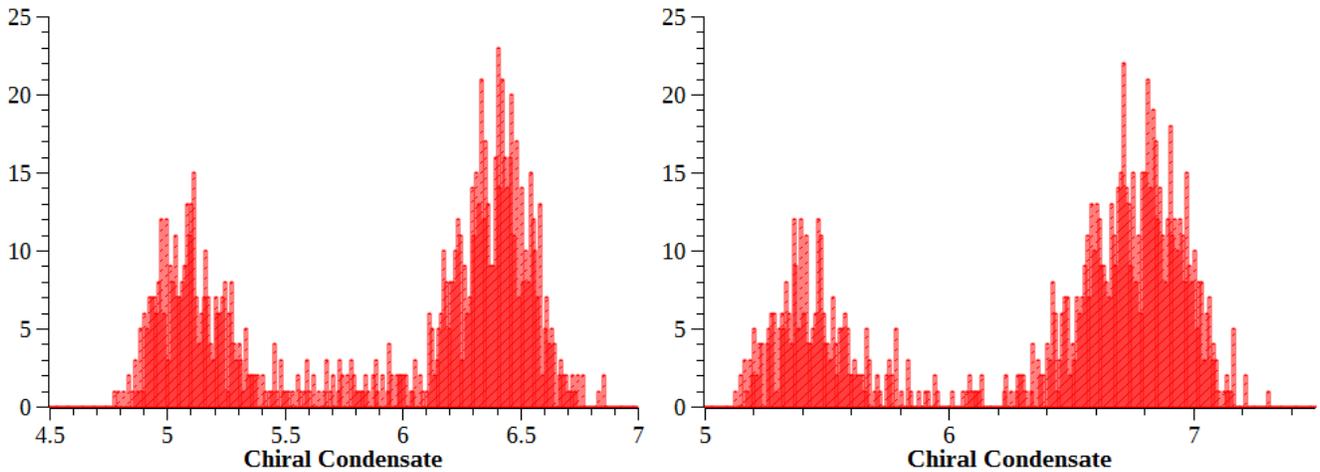

Fig. 6.22: Histograms of the chiral condensate for m_{scalar}=0.05; α=0.7 & κ=0.328 (left) and α=0.9 & κ=0.301 (right).

Further, if histograms of the chiral condensate for bare gaugino masses away from this point are considered, a first-order transition is indicated by the position of the peaks remaining constant. Figure 6.23 demonstrates this.

49
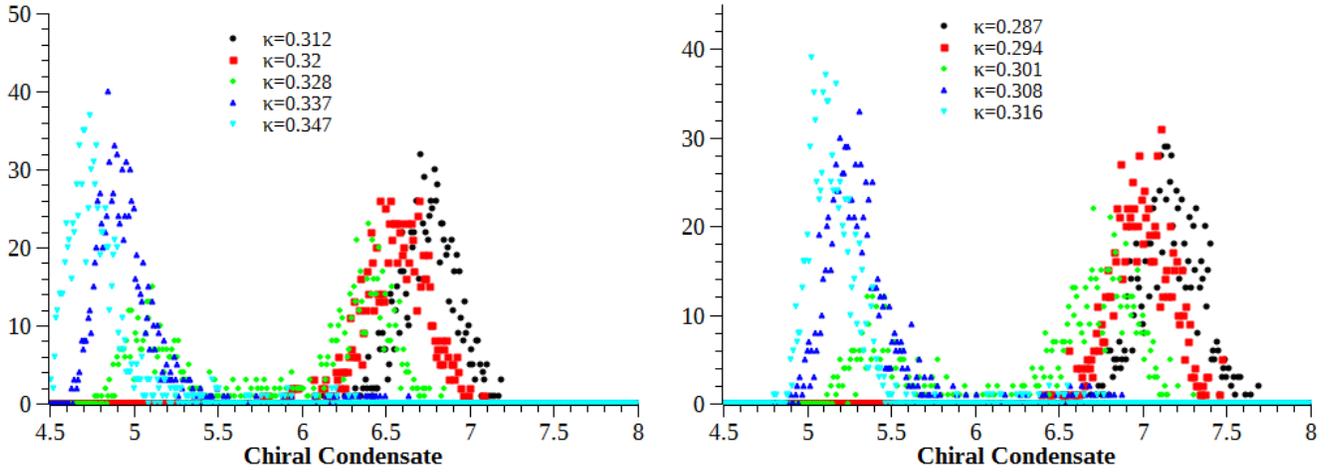
Fig. 6.23: Histograms of the chiral condensate for m_{scalar}=0.05; α=0.7 & κ=0.312, 0.32, 0.328, 0.337 & 0.347 (left) and α=0.9 & κ=0.287, 0.294, 0.301, 0.308 & 0.316 (right).

All of the above evidence, which verifies that a first-order transition takes place, points towards the spontaneous breaking of a symmetry. In [53], Banks & Casher linked the spontaneous breaking of chiral symmetry to the density of (near-)zero modes of the low-end spectrum of the Dirac operator. More simply, if the density of (near-)zero modes of the Dirac operator is non-zero, the chiral condensate is non-zero, implying a spontaneous breaking of chiral symmetry. However, it must be mentioned that this relation is mostly discussed for theories with gauge+fermion content. The literature seems to be lacking in information on what happens once scalars are introduced. Also, the relation is perfectly valid in the continuum limit, which means usage of larger lattices yields more accurate results. Keeping these two points in mind, preliminary results are presented in figures 6.24 and 6.25.
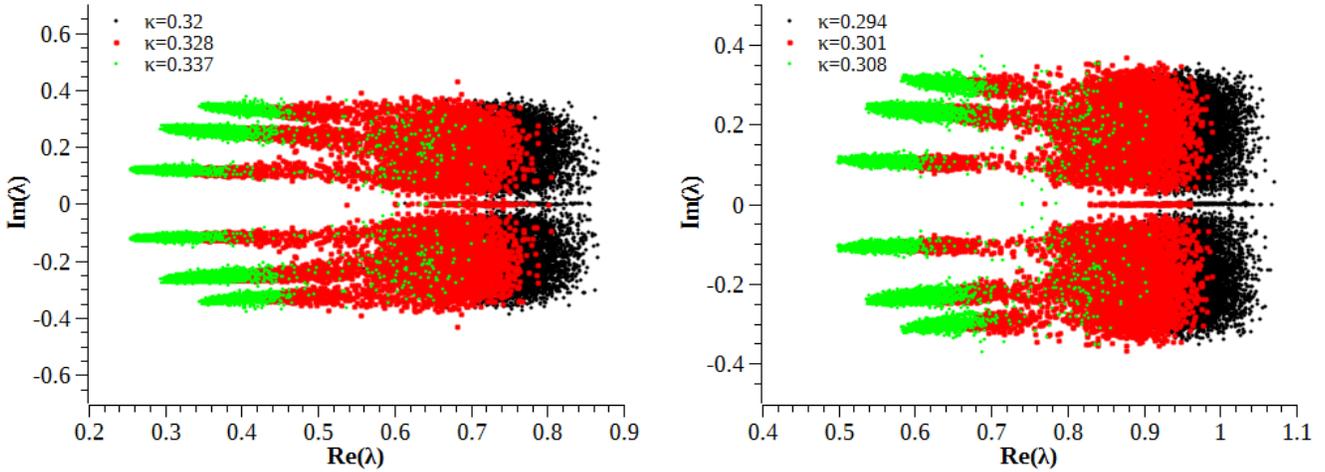
Fig. 6.24: The real and imaginary parts of lowest eigenvalues (λ) of the Dirac operator for m_{scalar}=0.05 on the 16x16 lattice for α=0.7 & κ=0.32, 0.328 & 0.337 (left) and α=0.9 & κ=0.294, 0.301 & 0.308 (right).
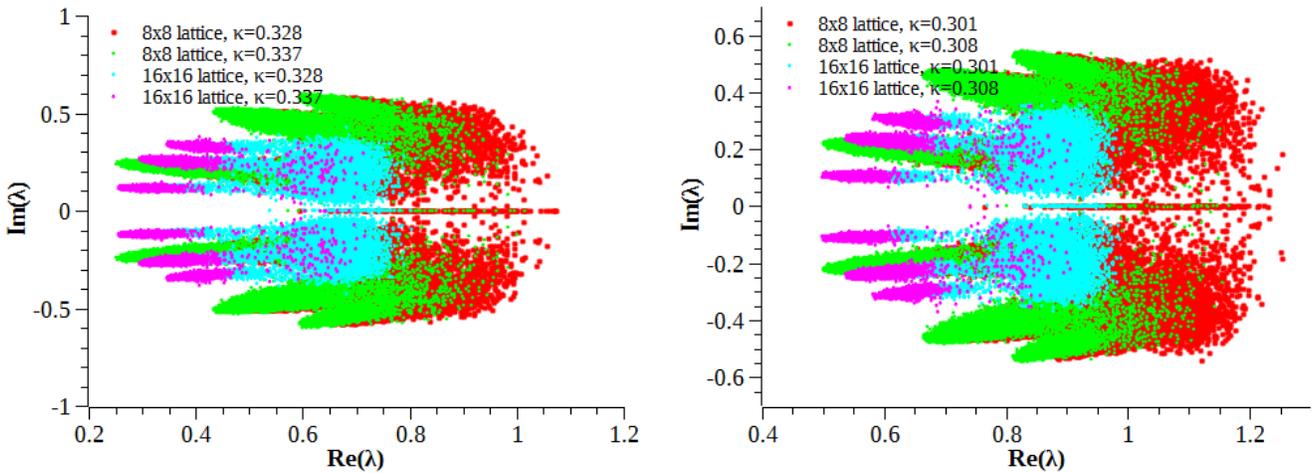

Fig. 6.25: A comparison of the lowest eigenvalues (λ) of the Dirac operator for m_{scalar}=0.05 on the 8x8 and 16x16 lattice for α=0.7 & κ=0.328 & 0.337 (left) and α=0.9 & κ=0.301 & 0.308 (right).

These are the hand/finger diagrams of the Dirac eigenvalues. From figures 6.24 and 6.25, the eigenvalues do move closer to 0 for larger lattices, but due to the restriction of the settings used, accurate calculations could not be carried out.

This behavior is displayed for lower scalar masses as well, although no corresponding loop or evidence of a first-order transition is seen. Figure 6.26 shows the eigenvalues of the Dirac operator for a scalar mass of 0.01.

51
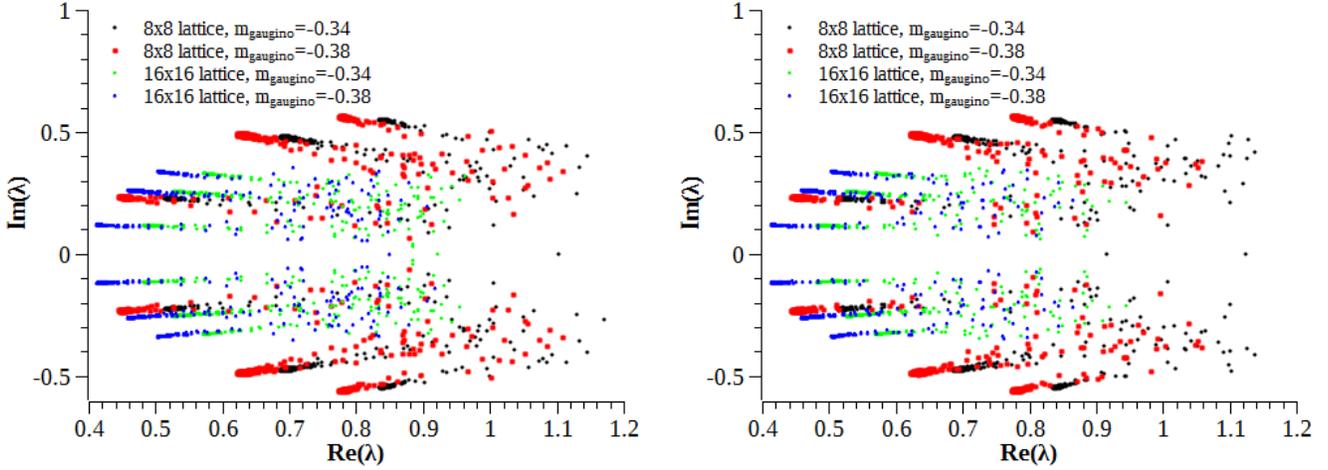
Fig. 6.26: A comparison of the lowest eigenvalues (λ) of the Dirac operator for m_{scalar}=0.01 on the 8x8 and 16x16 lattice for α=0.7 and κ=0.301 & 0.308 (left) and α=0.9 and $m_{gaugino}$=0.301 & 0.308 (right).

The eigenvalues still tend towards 0 in both cases. The difference between the figures for the two scalar masses is that in the case of m_{scalar}=0.01, the eigenvalues are more defined, whereas those in the case of m_{scalar}=0.05 are spread out.

Do the eigenvalues behave similarly in the case of the other transition in the chiral condensate? Figures 6.27 and 6.28 examine this for m_{scalar}=0.01 and 0.05.
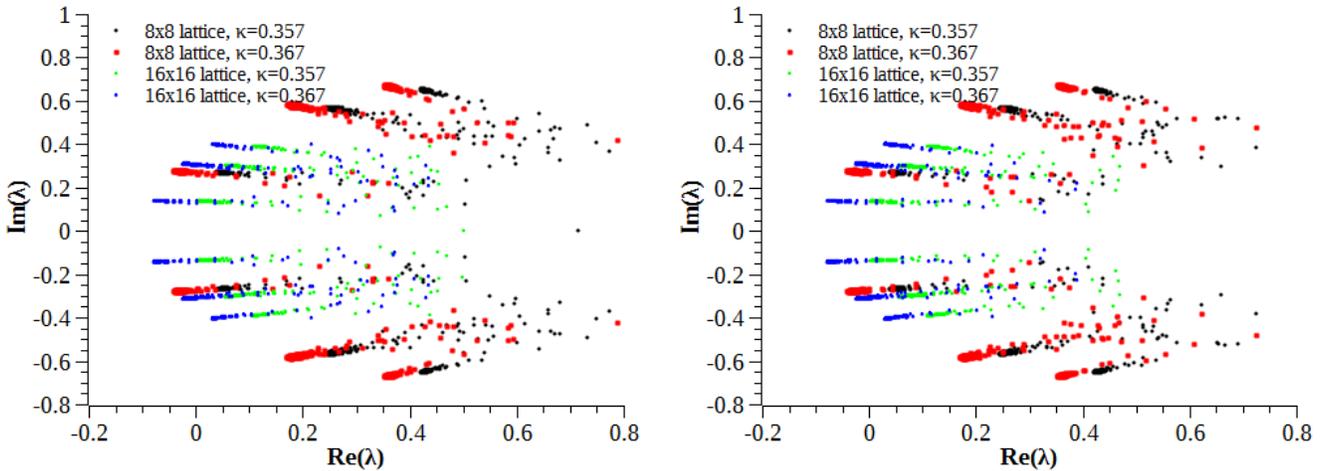

Fig. 6.27: A comparison of the lowest eigenvalues (λ) of the Dirac operator for m_{scalar}=0.01 on the 8x8 and 16x16 lattice for α=0.7 and κ=0.357 & 0.367 (left) and α=0.9 and $m_{gaugino}$=0.357 & 0.367 (right).
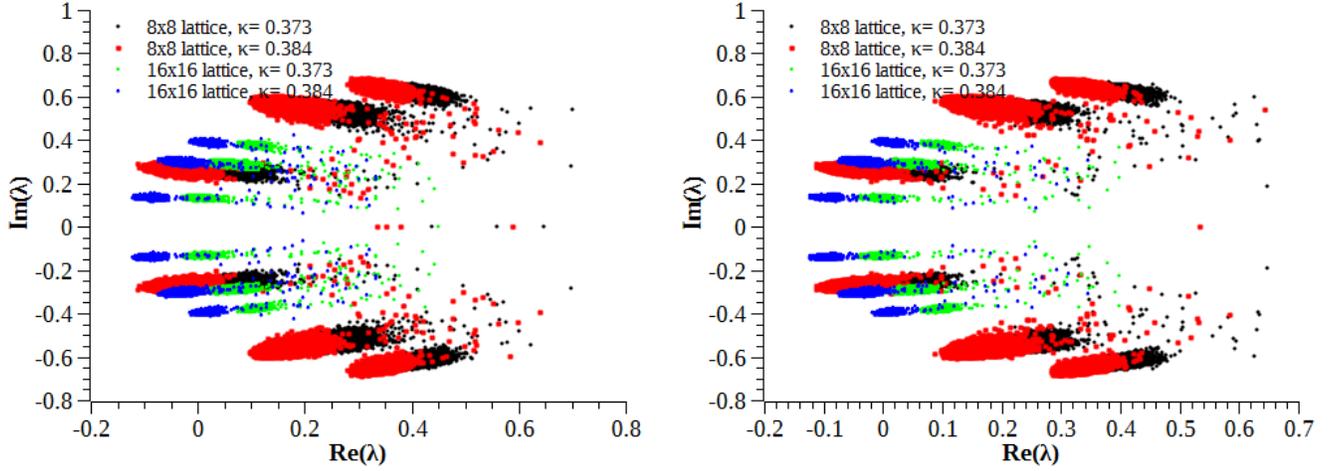
Fig. 6.28: A comparison of the lowest eigenvalues (λ) of the Dirac operator for m_{scalar}=0.05 on the 8x8 and 16x16 lattice for α=0.7 and κ=0.373 & 0.384 (left) and α=0.9 and $m_{gaugino}$=0.373 & 0.384 (right).

The comparatively diffuse nature of the eigenvalues for m_{scalar}=0.05 is also seen in this case. For both scalar masses, the eigenvalues bend towards proper 0 for larger lattices.

It is difficult to draw accurate conclusions from the available data. To check the bending of the eigenvalues towards 0 and calculate the density of (near-)zero modes and hence the chiral condensate, more lattices have to be used. The diffuseness of the eigenvalues for m_{scalar}=0.05 could be another clue towards a broken symmetry, since a symmetry transformation of the eigenvalues may not lead to a switch to a different branch/finger. In contrast, the sharp definition of the eigenvalues for m_{scalar}=0.01 makes it more probable that this would happen. Further simulations with intermediate scalar masses are necessary.

7. Summary, discussion and future prospects

Let us examine the simulation parameters and how they have affected the results.

The coupling parameter α is our first stop. A continuum limit can be obtained by writing

$$\alpha = \frac{V_{2D}}{g_{4D}^2} = \frac{(Na)^2}{g_{4D}^2} \tag{126}$$

N being the number of lattice points and a, the lattice spacing. This is trivial in 4D, but because the theory being studied has been derived from the 4D theory by dimensional compactification, the two compactified dimension can be thought of as being much smaller than the physical dimensions, validating the expression in 2D as well. Following this, the volume $V_{2D}=(Na)^2$ can be kept fixed. If larger and larger lattices are then used, i.e. $N \to \infty$, then $a \to 0$ necessarily.

The critical point of vanishing effective gaugino mass was successfully extracted using the transition in the chiral condensate and the linear extrapolation of the square of the pion mass to zero. The results are repeated below:

Using the chiral condensate: κ_C(8x8)=0.3709(7)   and κ_C(16x16)=0.3695(7)
Using the square of the pion mass: κ_C(16x16)=0.358(2)

The agreement between the values obtained using the two methods is good; there is a 3% difference between them, so both methods can be used to obtain a supersymmetric continuum limit. A comparison of these results can be done with the bosonic Ward identity (figure 6.12), where the average bosonic action is expected to be 5.5 at the critical value. Although this does not happen exactly, it is observed that the critical point at which the action density is 5.5 shifts closer to the values obtained using the chiral condensate and pion mass for increasing α, i.e. towards the continuum limit, where the Ward identity is satisfied exactly. The discrepancy is probably due to finite size effects and lattice artifacts.

The nature of the transition in the chiral condensate at the point of vanishing effective gaugino mass is not clear. It shows no signs of being a first-order transition. To compare with figure 6.17, which shows a first-order transition, the chiral condensate as a function of HMC time for the critical value of

the bare gaugino mass is shown below, in figure 7.1.
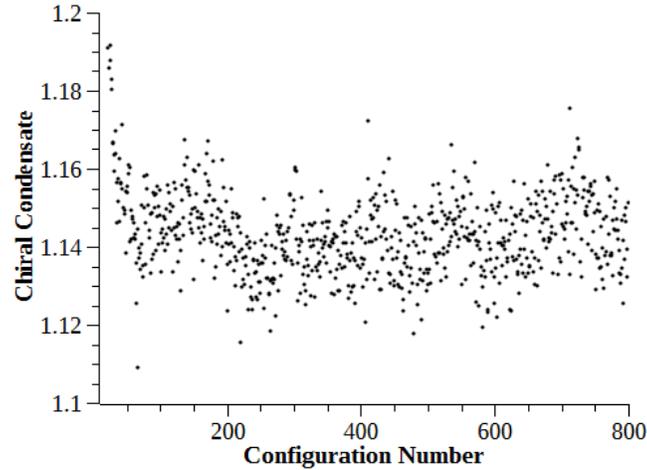
Fig. 7.1: The chiral condensate as a function of configuration number for α=0.9 and κ=0.357 on the 16x16 lattice.

One can only say that there may be a second-order transition here, but even this is unclear. In order to clear this up, the chiral susceptibility was calculated on both lattices, using finite differences. Forward, backward and central differences were calculated and then averaged over. Since, for a first-order transition, the peak should scale proportionate to the volume and for a higher-order transition, with a critical exponent, this could be a telling sign about the nature of the transitions. Figure 7.2 displays the susceptibility as a function of κ for different values of the scalar mass.
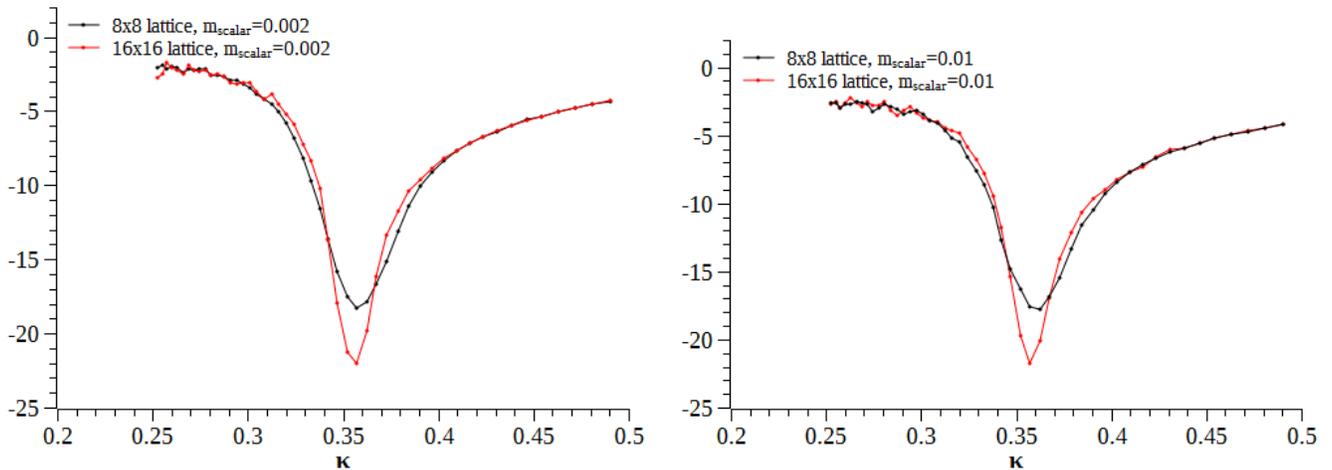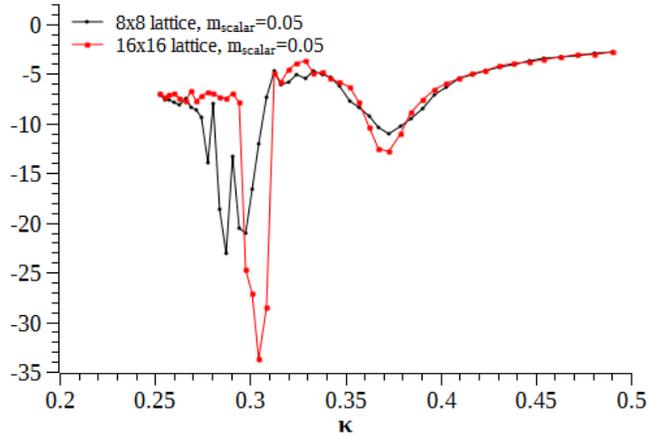
Fig. 7.2: The chiral susceptibility as a function of κ on both lattices for m_{scalar}=0.002 (previous page, left), 0.01 (previous page, right) & 0.05 (above).

Looking at the graph above, for a scalar mass of 0.05, there are clearly two peaks (the fluctuation on the 8x8 lattice is because of its smaller size). The larger peak on the left, at around κ=0.3 corresponds to the first-order transition that was observed and investigated earlier. The peak on the right, at κ~0.37 corresponds to the other transition. There is definitely a difference between the two, as can be observed from the scaling behavior. The peak on the left scales more strongly, whereas the peak on the right scales much more gently. Note the scaling of the right-side peak: the increase is O(3). Looking back at the chiral susceptibility curves for the lower scalar masses, this is also the scaling behavior displayed there. It seems that these are higher-order transitions, not first-order. In order to be sure about the scaling behavior, simulations on at least one more lattice size are necessary. If, in figure 7.2, the larger peak does represent a first-order transition, then, simulations on a 32x32 lattice should lead to a scaling similar to the one seen in the diagram. The critical exponent, which determines the scaling of the smaller peak, should then also reduce.

As a small aside, the determination of the critical value of κ at which the effective gaugino mass vanishes can also be determined using the chiral susceptibility. This would be a better signal because it is not affected by renormalization. In the continuum limit, however, the values obtained using this method and the transition of the chiral condensate will match. The improvement in the accuracy is especially noticeable for a scalar mass of 0.05. Consider the renormalized chiral condensate in this case (figure 6.16, reproduced here for the 16x16 lattice in figure 7.3):

56
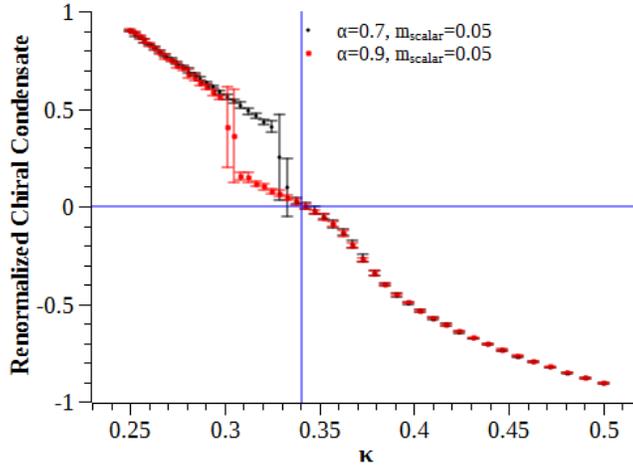
Fig. 7.3: The renormalized chiral condensate for m_{scalar}=0.05 α=0.7 and 0.9 as a function of κ on the 16x16 lattice.

The value of κ at which the chiral condensate vanishes is 0.3406(7), but this is clearly not the point at which the slope of chiral condensate changes (and, unfortunately, also not the point of the first-order transition). This point must be obtained by excluding the first-order transition and renormalizing that data, as shown in figure 7.4:
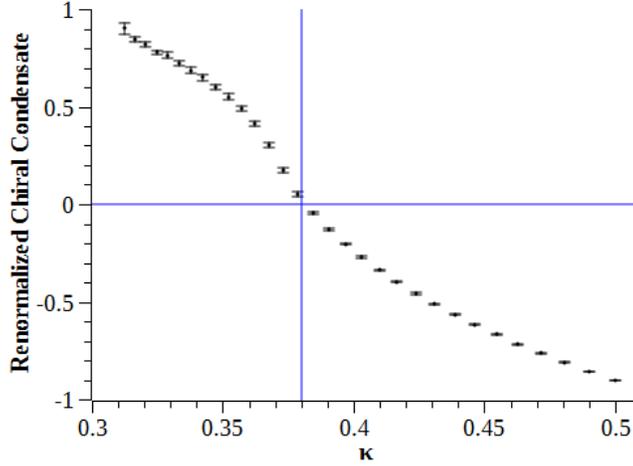
Fig. 7.4: The renormalized chiral condensate, excluding the first-order transition, for m_{scalar}=0.05 & α=0.9 on the 16x16 lattice.

From figure 7.4, the critical values of κ (at which the effective gaugino mass vanishes) can be obtained, which is 0.3801(7), which is very different from the value of vanishing chiral condensate. However, these two values should be the same, because in the chiral limit ($m_{gaugino} \rightarrow 0$), the chiral susceptibility

should diverge/change[54]. Thus, it may be advisable to calculate the chiral limit using the chiral susceptibility. Here are the values of κ corresponding to zero effective gaugino mass/zero chiral condensate for all scalar masses using both methods (on the 16x16 lattice):

m_{scalar}	κ using renormalized chiral condensate	κ using chiral susceptibility
0.002	0.3674(7)	0.3570(7)
0.01	0.3695(7)	0.3577(7)
0.05	0.3406(7)/0.3801(7)	0.3704(7)

It has been argued earlier that for a scalar mass of 0.05, the chiral condensate shows clear signs of a first-order transition. What causes this transition, spontaneous chiral symmetry breaking? In the last part of Section 6.7, preliminary data obtained for the investigation of the Banks-Casher relation was presented. As mentioned in that section, the lowest eigenvalues of the Dirac operator do show signs of behavior concordant with an agreement with the Banks-Casher relation: they extend towards the imaginary axis for larger bare gaugino masses and they also bend towards zero for larger volumes. If such a trend continues for larger lattices, a calculation of the density of these (near-)zero modes would give the value of the chiral condensate. If this is non-zero, then chiral symmetry is spontaneously broken. As was mentioned, further simulations on larger lattices are required for this.

There seems to be an interplay between the bare gaugino mass/κ and the scalar mass. A phase diagram of the theory in the scalar mass-bare gaugino mass plane would clarify this. Using the values in the table above, a diagram as in figure 7.5 can be drawn.
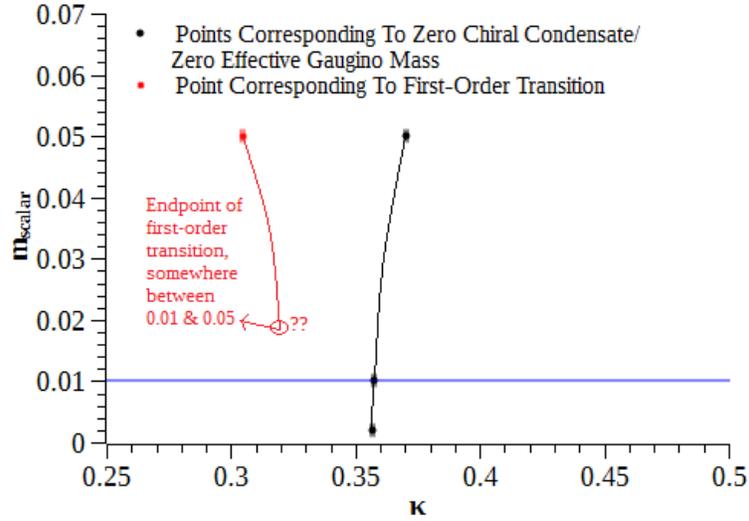
Fig. 7.5: The phase diagram of the theory under investigation using available data.

Along the black curve, the chiral condensate is zero and the effective gaugino mass is zero, which means this curve represents the chiral limit. It may be that this curve also represents the curve of supersymmetry restoration. Simulations with better statistics would enable the investigation of the bosonic Ward identity. If the bosonic action density crosses 5.5 at the values on this curve, it would increase the probability that it is. Other Ward identities could also be examined to increase confidence in this conclusion. The red point is what is known now about the first-order transition: for a scalar mass of 0.05, it happens for $\kappa = 0.3047(7)$. Since no such transition is observed for $m_{scalar} \leq 0.01$, it is estimated that at and above some critical scalar mass $0.01 \leq m_{critical} \leq 0.05$, there is a first-order transition. The red curve in figure 7.5 is purely qualitative and hypothetical. Simulations with a number of scalar masses between 0.01 and 0.05 will enable a determination of this critical mass.

Further, the cause of this first-order transition is not clear from the present simulations. As mentioned earlier, simulations on larger lattices would clarify the behavior of the eigenvalues of the Dirac operator. It could then be checked whether the Banks-Casher relation is satisfied and if spontaneous chiral symmetry breaking is responsible for this transition.

Bibliography

[1] C.N. Yang and R.L. Mills, Phys. Rev. **96**, 191 (1954).

[2] S. Weinberg, Phys. Rev. Lett. **19**, 1264 (1967).

[3] D.P. Barber, U. Becker, H. Benda, A. Boehm, J.G. Branson, J. Bron, D. Buikman, J. Burger, C.C. Chang, H.S. Chen, M. Chen, C.P. Cheng, Y.S. Chu, R. Clare, P. Duinker, G.Y. Fang, H. Fesefeldt, D. Fong, M. Fukushima, J.C. Guo, A. Hariri, G. Herten, M.C. Ho, H.K. Hsu, T.T. Hsu, R.W. Kadel, W. Krenz, J. Li, Q.Z. Li, M. Lu, D. Luckey, D.A. Ma, C.M. Ma, G.G.G. Massaro, T. Matsuda, H. Newman, J. Paradiso, F.P. Poschmann, J.P. Revol, M. Rohde, H. Rykaczewski, K. Sinram, H.W. Tang, L.G. Tang, S.C.C. Ting, K.L. Tung, F. Vannucci, X.R. Wang, P.S. Wei, M. White, G.H. Wu, T.W. Wu, J.P. Xi, P.C. Yang, X.H. Yu, N.L. Zhang, and R.Y. Zhu, Phys. Rev. Lett. **43**, 830 (1979).

[4] ATLAS Collaboration, Science **338**, 1576 (2012).

[5] J.W.F. Valle, in *AIP Conf. Proc.* (2005), pp. 128–134.

[6] L. Canetti, M. Drewes, and M. Shaposhnikov, New J. Phys. **14**, 095012 (2012).

[7] V. Trimble, Annu. Rev. Astron. Astrophys. **25**, 425 (1987).

[8] S. Coleman and J. Mandula, Phys. Rev. **159**, 1251 (1967).

[9] R. Haag, J.T. Łopuszański, and M. Sohnius, Nucl. Phys. B **88**, 257 (1975).

[10] S. Dimopoulos and H. Georgi, Nucl. Phys. B **193**, 150 (1981).

[11] G. Hiller and M. Schmaltz, Phys. Lett. B **514**, 263 (2001).

[12] G. Jungman, M. Kamionkowski, and K. Griest, Phys. Rep. **267**, 195 (1996).

[13] G. Bertone, D. Hooper, and J. Silk, Phys. Rep. **405**, 279 (2005).

[14] K. Wilson, Phys. Rev. D **10**, 2445 (1974).

[15] S. Dürr, Z. Fodor, J. Frison, C. Hoelbling, R. Hoffmann, S.D. Katz, S. Krieg, T. Kurth, L. Lellouch, T. Lippert, K.K. Szabo, and G. Vulvert, Science **322**, 1224 (2008).

[16] P.H. Dondi and H. Nicolai, Nuovo Cim. A **41**, 1 (1977).

[17] H.B. Nielsen and M. Ninomiya, Phys. Lett. B **105**, 219 (1981).

[18] P. Ginsparg and K. Wilson, Phys. Rev. D **25**, 2649 (1982).

[19] J.-L. Gervais and B. Sakita, Nucl. Phys. B **34**, 632 (1971).

[20] Y.A. Gol'fand and E.P. Likhtman, JETP Lett. **13,** 323 (1989).

[21] D.V. Volkov and V.P. Akulov, JETP Lett. **16**, 438 (1972).

[22] J. Wess and B. Zumino, Nucl. Phys. B **70**, 39 (1974).

[23] M.F. Sohnius, Phys. Rep. **128**, 39 (1985).

[24] W. Nahm, Nucl. Phys. B **135**, 149 (1978).

[25] A. Salam and J. Strathdee, Nucl. Phys. B **76**, 477 (1974).

[26] S. Ferrara, B. Zumino, and J. Wess, Phys. Lett. B **51**, 239 (1974).

[27] R. Feynman, Rev. Mod. Phys. **20**, 367 (1948).

[28] G. Münster and M. Walzl, arXiv:hep-lat/0012005 (2000).

[29] M. Lüscher, Nucl. Phys. B **478**, 365 (1996).

[30] F. Fucito, E. Marinari, G. Parisi, and C. Rebbi, Nucl. Phys. B **180**, 369 (1981).

[31] I.L. Horváth, S. Sint, and A.D. Kennedy, Nucl. Phys. B, Proc. Suppl. **73**, 834 (1999).

[32] M. Bochicchio, L. Maiani, G. Martinelli, G. Rossi, and M. Testa, Nucl. Phys. B **262**, 331 (1985).

[33] G. Curci and G. Veneziano, Nucl. Phys. B **292**, 555 (1987).

[34] R. Kirchner, S. Luckmann, I. Montvay, K. Spanderen, and J. Westphalen, Nucl. Phys. B - Proc. Suppl. **73**, 828 (1999).

[35] I. Campos et al., Eur. Phys. J. C **11**, 507 (1999).

61

[36] F. Farchioni, A. Feo, T. Galla, C. Gebert, R. Kirchner, I. Montvay, G. Münster, and A. Vladikas, Nucl. Phys. B - Proc. Suppl. **94**, 787 (2001).

[37] F. Farchioni, A. Feo, T. Galla, C. Gebert, R. Kirchner, I. Montvay, G. Münster, and A. Vladikas, (2001).

[38] M. Lüscher, Report for 49e Ecole d'Eté de Physique Théorique, Les Houches, 451-528 (1988)

[39] S. Aoki, T. Umemura, M. Fukugita, N. Ishizuka, H. Mino, M. Okawa, and A. Ukawa, Phys. Rev. D **50**, 486 (1994).

[40] M.H. Quenouille, Math. Proc. Cambridge Philos. Soc. **45**, 483 (2008).

[41] J.W. Tukey, in *Ann. Math. Stat.* (1958), p. 614.

[42] S. Duane, A.D. Kennedy, B.J. Pendleton, and D. Roweth, Phys. Lett. B **195**, 216 (1987).

[43] E.Y. Remez, Comm. Soc. Math. Kharkov **10**, 41 (1934).

[44] B. Jegerlehner, arXiv:hep-lat/9612014 (1996).

[45] J. Scherk and J.H. Schwarz, Phys. Lett. B **57**, 463 (1975).

[46] L. Brink, J.H. Schwarz, and J. Scherk, Nucl. Phys. B **121**, 77 (1977).

[47] A. FEO, Mod. Phys. Lett. A **19**, 2387 (2004).

[48] A. Donini, M. Guagnelli, P. Hernandez, and A. Vladikas, Nucl. Phys. B **523**, 529 (1998).

[49] G. Veneziano and S. Yankielowicz, Phys. Lett. B **113**, 231 (1982).

[50] F. Farchioni et al., Eur. Phys. J. C - Part. Fields **23**, 719 (2002).

[51] S. Catterall, arXiv:hep-lat/0602004 (2006).

[52] B.-H. Wellegehausen, Phase diagrams of exceptional and supersymmetric lattice gauge theories, PhD thesis, Jena (2012).

[53] T. Banks and A. Casher, Nucl. Phys. B **169**, 103 (1980).

[54] J. Trampetic and J. Wess, Particle Physics in the New Millennium: Proceedings of the 8th Adriatic Meeting, Band 1 (2003).

Sworn statement

I declare that I have researched and written this Master thesis myself. No passages of text have been taken from third parties without being identified as such and all tools and sources have been indicated in the thesis. No third party has received any monetary benefits for work in connection with this thesis.

This Master thesis has not yet been submitted as an examination paper for state or other academic examinations.

Jena, 27.11.2014   Suraj Krishnamurthy

Acknowledgment

My first wish of thanks must go to Prof. Wipf for giving me this opportunity to learn about what was, at the time, essentially 2 fields that were new to me: supersymmetry and lattice gauge theory, and for allowing me to perform my thesis on these subjects in his research group.

Dr. Wellegehausen deserves my deepest vote of thanks. I have troubled him with what must have been the most basic questions, but he always patiently clarified things for me. This thesis would have taken a lot longer to complete if I did not have the advantage of his advice and help.

On another note, I must thank Prof. Schäfer, whom I knew in his capacity as the Dean at the Examination Office for the Physics & Astronomy department. If it wasn't for his support, I would not have been able to come to Jena to study.

Of course, I owe my parents a whole lot, not least of all for their support and their surprisingly constant interest in what I was studying here.

Curriculum Vitae

Name: Suraj Krishnamurthy

Birth date: 01.01.1989

Place of birth: Bangalore, India

Education:

1994-2004: High school education at The Frank Anthony Public School, Bangalore

2004-2006: Pre-university education at Shri Bhagawan Mahaveer Jain College, Bangalore

2006-2009: B.Sc. in physics, mathematics and computer science at Shri Bhagawan Mahaveer Jain College, Bangalore

2009-2011: M.Sc. in physics with a specialization in materials science at the Center for Post-Graduate Studies, Jain University, Bangalore

2012-2013: One year of M.Sc. course studies in physics at Universität Siegen, Siegen.

2013-2014: Continuation of M.Sc. in physics and Master thesis at Friedrich-Schiller-Universität, Jena.